

UC Santa Barbara

NCGIA Technical Reports

Title

Image Registration using Multiquadric Functions, the Finite Element Method, Bivariate Mapping Polynomials and Thin Plate Spline (96-1)

Permalink

<https://escholarship.org/uc/item/8kg6w8fv>

Authors

Fogel, David N.
Tinney, Larry R.

Publication Date

1996-03-01

NCGIA

**National Center for
Geographic Information and Analysis**

**Image Registration using
Multiquadric Functions, the Finite Element
Method, Bivariate Mapping Polynomials and
Thin Plate Spline**

by

David N. Fogel
University of California, Santa Barbara

Larry R. Tinney
DOE Remote Sensing Laboratory, Las Vegas

Technical Report 96-1

March 1996

**Simonett Center for Spatial Analysis
University of California**
35 10 Phelps Hall
Santa Barbara, CA 93106-4060
Office (805) 893-8224
Fax (805) 893-8617
ncgia@ncgia.ucsb.edu

State University of New York
301 Wilkeson Quad, Box 610023
Buffalo NY 14261-0001
Office (716) 645-2545
Fax (716) 645-5957
ncgia@ubvms.cc.buffalo.edu

University of Maine
348 Boardman Hall
Orono ME 04469-5711
Office (207) 581-2149
Fax (207) 581-2206
ncgia@spatial.maine.edu

Title:**Image Registration using Multiquadric Functions, the Finite Element Method, Bivariate Mapping Polynomials and the Thin Plate Spline****Authors and Affiliations:****David N. Fogel**

National Center for Geographic Information and Analysis
University of California, Santa Barbara
fogel@ncgia.ucsb.edu

Larry R. Tinney

Multispectral Remote Sensing and Geographic Information Systems
Bechtel Nevada
tinneylr@nv.doe.gov

Keywords:

image rectification, image registration, surface fitting, scattered data interpolation, triangulation, interpolation, approximation, bivariate mapping polynomials, multiquadrics, thin plate spline

Short Title:

Image Registration using Multiquadric Functions

Name and Address of Author for Correspondence:

Larry R. Tinney, Manager
Multispectral Remote Sensing and Geographic Information Systems
DOE Remote Sensing Laboratory
P.O. Box 98521, MS RSL-19
Las Vegas, Nevada 89193-8521
tinneylr@nv.doe.gov

Acknowledgments:

The authors wish to thank the following people for their generous assistance on technical issues addressed in an earlier version of this report: Manfred Ehlers (ISPA-University of Osnabrueck-Vechta, Germany), Albert L. Zobrist (Rand Corporation, Santa Monica, California), Waldo R. Tobler (University of California, Santa Barbara), Ian Barrodale (Barrodale Computing Services, Victoria, B.C., Canada), Robert P. Comer (TASC, Reading, Massachusetts) and Richard Franke (Naval Postgraduate School, Monterey, California).

Additionally, the authors wish to express their appreciation to Juliusz Ostrowski and Dave Stanley of PCI, and Brad Skelton and Brian Kloer of ERDAS for their helpful comments and suggestions. Of course, the authors take full responsibility for any errors contained herein.

Abstract

In this report, three methods of image-to-image registration using control points are evaluated. We assume that ephemeris sensor and platform data are unavailable. These techniques are the polynomial method, the piecewise linear transformation and the multiquadric method. The motivation for this research is the need for more accurate geometric correction of digital remote sensing data. This is especially important for airborne scanned imagery which is characterized by greater distortions than satellite data.

The polynomial and piecewise linear methods were developed for use with satellite imagery and have remained popular due to their relative simplicity in theory and implementation. With respect to airborne data however, both of these methods have serious shortcomings. The polynomial method, a global model, is generally applied as a least-squares approximation to the control points. Mathematically it is unconstrained between points leading to undesirable excursions in the warp. The piecewise linear method (or finite element method), a local procedure, produces a faceted irregular warp when the distortions between the control points are highly nonlinear.

The multiquadric method is a radial basis function. Two radial basis functions show promise for image warping: the multiquadric and thin plate spline. The multiquadric method is a global technique which captures local variations and interpolates, passing through the control points. It includes a tension-like parameter which can be used to adjust its behavior relative to local distortions. The principal shortcoming of the multiquadric method is that it is quite computationally intensive. Both the multiquadric method and thin plate splines have been evaluated extensively for scattered data interpolation.

In a test application using badly warped aircraft imagery, the multiquadric method produced better results both visually, *e.g.* crooked lines were straightened, and quantitatively with lower residual errors. The results for the multiquadric method are encouraging for improved environmental remote sensing and geographic information systems integration. The technique may be applied to satellite data as well as to airborne scanner data. The multiquadric method may be used for warping polygons and applied to mosaicking as well. Its present functional form is flexible and may be modified quite easily to further adapt to local distortions, a task not performed for this report. Advances in the rapid evaluation of radial basis functions will make both the multiquadric and thin plate spline techniques even more attractive in the future.

1 Introduction

This report evaluates multiquadric functions for image registration and rectification of airborne scanner data. Two conventional registration techniques used in environmental remote sensing will be evaluated against the multiquadric method: bivariate mapping polynomials and the finite element method (piecewise linear). There are five sections in this report: (1) this introduction; (2) an overview of the geometric correction process; (3) a technical discussion of the three techniques under investigation; (4) the results of an experiment with a badly warped image; and (5) a final section providing a summary and recommendations for future research.

The motivation of this study stems from problems specific to the registration and rectification of airborne scanner acquired digital imagery. Conventional methods used for the registration of satellite imagery are not sufficiently robust to model the more complicated distortions found in airborne scanned imagery. The Department of Energy's Remote Sensing Laboratory (RSL), operated by EG&G Energy Measurements, is supporting this evaluation of Hardy's multiquadric functions for image warping. This project is a part of the Department of Energy (DOE) program involving the use of remote sensing technology for Environmental Restoration and Waste Management (ERWM).

The research is a collaborative effort between RSL, the Geographic Information Systems and Remote Sensing Laboratory at the Institute for Structural Planning in Areas of Intensive Agriculture (ISPA), Universität Osnabrück-Standort Vechta and the Remote Sensing Research Unit at the University of California, Santa Barbara (RSRU; UCSB). It constitutes a follow-up to previous RSL and RSRU cooperative research on geometric correction in conjunction with the National Center for Geographic Information and Analysis (NCGIA) Initiative (Scepan, Estes and Lanter 1992). NCGIA I-12 addresses the integration of Remote Sensing and Geographic Information Systems technologies (see "Special Issue: Integration of Remote Sensing and GIS," *Photogrammetric Engineering and Remote Sensing* LVII(6) 1991).

1.1 Background

Conventional techniques for earth remotely sensed image registration consist of surface fitting models: bivariate mapping polynomial functions and finite element methods. These techniques are in many cases adequate for images characterized by small systematic global distortions or local distortions, respectively. However, these techniques have not proved adequate for airborne scanner imagery that may contain rapidly varying, nonsystematic distortions. At the same time, new, more accurate methods are being demanded by the earth remote sensing community at large. Information-extraction techniques demand radiometric and geometric fidelity. In this report, we address the latter problem, although the two are fundamentally interrelated.

In the case of EG&G/RSL, the ability to accurately register imagery is of paramount importance for environmental monitoring of Department of Energy facilities. Misregistration effectively degrades image information content for multiple-sensor and multi-temporal analyses. It is important that new techniques be operationalized to improve image registration accuracy for change detection, classification problems and remote sensing/geographic information system (RS/GIS) integration. Improvements in distortion modeling would be akin to increasing the effective resolution of an integrated dataset. There will be potential to extract more information from precision-corrected airborne scanner data.

Image registration of remotely sensed imagery encompasses three related problems: (1) image overlay or image-to-image registration; (2) image rectification or image-to-map registration; and (3) image mosaicking. We limit ourselves to discussing the first problem. Image rectification and image mosaicking may be considered as extensions of image registration, albeit with a host of additional complications.

1.1.1 Project Objective

The objective of this report is to evaluate the suitability of the multiquadric method for airborne scanner image registration. This evaluation includes a technical discussion of the polynomial, piecewise linear and multiquadric methods. The characteristics of these methods are described and applied to a test case. The accuracy of the techniques is quantitatively established by measuring misregistration using the root mean squared error criterion. Finally, this report includes a brief discussion of implementation issues such as computational complexity and numerical analysis.

1.1.2 Project Participants

The evaluation of the multiquadric method for image registration involved cooperation among the three facilities: RSL, ISPA and RSRU. RSRU coordinated the research, providing monthly progress reports and overseeing the preparation of this final report. The following persons and organizations participated in this joint research project:

Larry R. Tinney, Manager
Spectral Imaging and Geographic Information Systems
Remote Sensing Laboratory
EG&G Energy Measurements
P.O. Box 1912, MS RSL-19
Las Vegas, Nevada 89125

Dr. John E. Estes, Professor of Geography
Joseph Scepan
David N. Fogel
Remote Sensing Research Unit (RSRU)
Department of Geography
University of California
Santa Barbara, California 93106-4060

Dr. Manfred Ehlers, Professor for GIS and Remote Sensing
Uwe Flottemesch
David R. Steiner
Institute for Structural Research and Planning in Areas of Intensive Agriculture (ISPA)
University of Osnabrueck-Vechta
P.O. Box 1553, D-49364 Vechta, Germany

1.1.3 Project Overview

A series of general tasks for each participant was outlined to complete this project. The principal contributions are listed below:

- ISPA implemented the multiquadric method for image registration in the C programming language (ANSI C) and provided additional technical material to aid EG&G/RSL and RSRU in the writing of this report.
- EG&G/RSL provided a set of imagery for testing that consisted of badly distorted airborne scanned imagery and a set of reference aerial photographs.
- RSRU compiled detailed technical information on the techniques and conducted a test using the test imagery from EG&G/RSL.

1.2 Report Outline

There are three principal components in this report in addition to the summary and conclusions. The original work statement called for a short, summarizing technical document. However, during the course of the literature review for this project, it became apparent that many aspects of the image registration problem are not well understood. Therefore, we have chosen to elaborate on the problems and potential for modeling geometric correction as a step to aid technology transfer of this basic research to the earth remote sensing community.

In the section, *Image Registration and Image Rectification*, we describe the nature of image distortions, discuss geometric correction techniques in general and review numerous important concepts. This is a necessary prelude to subsequent technical discussions in the section.

The next section, *Surface Fitting Models*, includes a brief technical description of the two most commonly used geometric correction methods as well as an introduction to the class of functions to which the multiquadric method belongs. In this section, numerous observations are made with respect to the features characterizing each of the methods. We note that there is substantial room for improvement over current practice.

The performance of these techniques, that is how well each method corrected for geometric distortions, is described in the section, *Las Vegas Experiment*. The experiment, though limited to a single image set, provides us with an opportunity to empirically describe (using images, tables and graphics), that which has been reviewed only in conceptual and technical terms. We have chosen as a matter of convenience to include the images and the graphics in numerous separate appendices. Extensive references to the appendices are made throughout this section.

Finally, there is a short discussion on the implications of this research. The discussion focuses not only on the multiquadric method, but on image registration practices in general. Recommendations for improved geometric correction are also provided.

2 Image Registration and Image Rectification

In this section we provide an overview of those concepts most important to understanding the image registration problem. We feel the presentation is necessary given the limited amount of recent attention to the registration problem by the Earth remote sensing community. In fact, advances in the area of digital image manipulation are found mainly in the area of computer science and computer graphics.

2.1 Warping and Resampling

Modeling the deformation between images must address both locational attributes of a pixel and the corresponding numerical values. Deriving a mathematical expression for an image-to-image transformation is the first step in image warping. The second step involves the computation of new pixel values for the output image geometry. This is a problem of pixel value interpolation commonly termed image resampling. The most common resampling functions are nearest neighbor, bilinear and bicubic interpolation.

There are trade-offs with each of these approaches. For example it is commonly known that bicubic interpolation or cubic convolution may underestimate or overestimate the pixel values distorting the radiometric characteristics of the imagery. This may confound subsequent analyses. Image and application idiosyncrasies determine which interpolation method is best. The nearest neighbor approach is generally used when radiometric fidelity is at a premium. However, bilinear interpolation and cubic convolution yield more visually pleasing results and in many cases cubic convolution is an acceptable technique. There is a free parameter in cubic convolution that is often set to -1.0 or -0.5 that is rarely discussed in remote sensing, but profoundly affects the results. At the same time, it is rarely made clear whether interpolated values are rounded or truncated by scientists or in application software documentation.

More sophisticated and computationally intensive interpolations functions are known. The interpolation literature is vast and will not be detailed here. We focus on the mathematical modeling of the pixel locations. It is sufficient to point out that more complex resampling functions have been developed and that this is an active research area. Introductory discussions may be found in Bernstein (1983), Mather (1987), Moik (1980), Simon (1975) and Swartzlander *et al.* (1988).

2.2 Distortions

Geometric distortions, or error, in remotely sensed satellite imagery can be categorized as either internal (sensor-related) or external (platform perturbations and scene characteristics). Internal distortions include, but are not limited to centering, scale and skew effects. External distortions include attitude effects, altitude deviations, earth curvature and the viewing geometry. Landsat and SPOT imagery are characterized

by low-frequency (smoothly varying) distortions. As such the imagery may be corrected using relatively simple mathematical models. Airborne scanner imagery exhibits additional geometric distortion due to aircraft vibration, flightline drift and changes in velocity as well as much greater topographic effects. The internal and external geometric error found in imagery acquired by airborne scanners must be modeled by more sophisticated methods.

More information on geometric distortion may be found in Moik (1980), Bryant (1982), Bernstein (1983) and Billingsley (1983). Image geometry properties related to remotely sensed imagery as well as digital images in general may be found in Wolberg (1990).

2.3 Spatial Transformations

There are three principal concepts specific to image warping which merit discussion for the remote sensing specialist. These involve how well-identified pairs of matched points are registered (interpolation and approximation), the direction of the mapping function (forward or inverse mapping) and the nature of the mathematical modeling techniques (local or global).

We review these ideas to establish the background for this report and to clarify terminology. In general, a distortion model is sensor and scene dependent. The concepts below describe technical issues surrounding the development of distortion models and provide some explanations for conventional practice.

2.3.1 Interpolation and Approximation

In the context of image registration for remote sensing, the polynomials and finite element methods approximate and interpolate, respectively. We use the term *approximation* to denote that the mapping function approximately models the fit of the control points. Polynomials only interpolate if the system of equations is strictly determined. If however, the number of control points is such that we have an overdetermined system of equations, the polynomials approximate the locations of the control points. Common practice is to select many control points using a least-squares fit to characterize the geometric distortions, thus specifying an approximating model.

The finite element method is an interpolating procedure that means that the geometric distortion model passes through the control points. It is clear that *interpolation* is a desirable feature, especially for data with high spatial resolution where distinctive features can be readily identified.

2.3.2 Forward and Inverse Mapping

Geometric transformations of images involve developing a correspondence between the input and output images. This geometric relationship may be expressed by either a forward mapping or an inverse mapping. In remote sensing applications, the general practice is to develop an inverse mapping. The reasons for this will become clear after we describe forward mapping and its inherent shortcomings.

In a forward mapping, the output coordinates are found as a function of the input coordinates. There are two fundamental shortcomings to using this technique. First, it is possible to map many points of the input image on to a single point in the output image. These may be viewed as overlaps. Second, it is possible to have areas of undefined pixels, or holes, in the output image where no pixels were mapped from the input on to the output image. These are not insurmountable obstacles. However, additional operational problems are introduced in the resampling process increasing the complexity of the registration problem. This is basically an implementation issue, though there are theoretical considerations as well.

Inverse mapping avoids the problems of holes and overlaps by mapping the output image onto the input image. This initially appears to be counter-intuitive. However, the mapping of each output coordinate onto an input coordinate ensures a continuous output image devoid of holes and overlaps. Still, inverse mappings may lose information similar to the problem of holes occasionally found in forward mappings. The inverse mapping of pixel values is confounded if the distortion model does not adequately fit, or completely sample the input image. In other words, the geometric model in combination with the resampling method may

not reference every single pixel in the input image. Therefore the output image potentially has less information as a result of model mis-specification and resampling errors.

2.3.3 Global and Local Methods

A global transformation simply means that all the control points are used to derive a single mathematical model of the geometric distortions. Local methods use subsets of the data and as such derive many distortion models. The distinction may be blurred. For example, if we were to use distance-weighted polynomials, a global procedure, the local distortions will be incorporated to some degree in the mathematical model. A different case arises with the local weighted mean procedure. This is a local model, but we must still quantify the concept of proximity to operationalize the technique. Finally, it must be recognized that the local fitting procedures require a tessellation of the control points which in effect influences the model parameters.

2.4 Sensor Modeling

Modeling geometric distortions using ephemeris sensor data is a traditional approach in photogrammetry. Analytical or parametric models may also be applied to satellite data without too much difficulty. More difficult, but still possible, is to collect airborne sensor-specific information using advanced position and attitude measuring systems, such as differential GPS (Global Positioning System) and INS (Inertial Navigation System) technology.

Although significant advances are being made in this area, these techniques are not addressed in this report. Full implementations of these ephemeris methods are currently expensive though they hold great promise for automatic correction of systematic geometric distortions. Indeed, the further integration into these models of ground control information in the form of digital elevation models is an important research area.

The registration methods and issues discussed here will remain applicable for fine tuning ephemeris-corrected data. These methods will also be effective at registering historical data and new imagery acquired without the benefit of ephemeris data.

2.5 Surface Fitting

The development of a geometric distortion model using control points may be considered an exercise in surface fitting. These are numerical, rather than parametric, approaches. The polynomial, finite element, and multiquadric method are all surface fitting models. It is possible to derive hybrid models using a combination of analytic and numerical approaches. Such hybrid approaches, however, are beyond the scope of this investigation. The following section addresses surface fitting models in more detail.

3 Surface Fitting Techniques

This section describes three surface fitting methods: bivariate mapping polynomials, finite element methods and radial basis function methods. The first two topics correspond to those methods most frequently used in remote sensing, *i.e.* power series polynomials and the piecewise linear finite element method. The multiquadric method belongs to the family of radial basis functions. A second radial basis function, the thin plate spline, is also discussed.

3.1 Bivariate Mapping Polynomials

The most widely used approach for correcting the geometry of remotely sensed imagery is based on procedures that make use of polynomial power series. Polynomial methods may be interpolating or approximating functions depending on the number of control points. An interpolation condition exists when the number of control points is equal to the number of unknown terms in the polynomial expression. The system of equations is said to be fully determined. In the interpolation case, the control points are mapped exactly from the output space to the input space. For example, identified road intersections will be mapped to road intersections and not to nearby locations; there is no residual distortion at each control point.

When the number of control points is greater than the number of unknown terms, the transformation coefficients are approximated. The control points will not be located in the same place by the distortion model. For example, a road intersection identified on an image may not map precisely to the same road intersection on the target or base image. In the approximating case, residual distortion typically exists at each control point. In some cases, the residual distortion may be negligible while in extreme cases the misregistration can be quite significant.

Polynomials higher than the first degree may result in unwanted or undesirable stretching or squeezing and perform badly at extrapolation. This is most obvious for polynomials of third degree and higher. For this reason, polynomial methods are best applied when the image distortions are slight. To avoid extrapolation problems with high order polynomials, it is best if the control points completely surround, or envelop the region of interest. Except for relatively small areas, the high frequency distortions in airborne scanner imagery are often too complicated to model adequately using polynomial power series.

The specification of a distortion model using polynomials is straightforward. Bivariate polynomial transformations in remote sensing are usually specified in the following form (*e.g.*, Moik 1980 and Wolberg 1990), where $x=f(u,v)$, $y=g(u,v)$ and N is the polynomial degree:

$$x = \sum_{i=0}^N \sum_{j=0}^{N-1} a_{ij} u^i v^j \quad (3-1)$$

and

$$y = \sum_{i=0}^N \sum_{j=0}^{N-1} b_{ij} u^i v^j \quad (3-2)$$

For $N=3$, the polynomial relationship may be expressed by:

$$x = a_{00} + a_{01}v + a_{02}v^2 + a_{03}v^3 + a_{10}u + a_{11}uv + a_{12}uv^2 + a_{20}u^2 + a_{21}u^2v + a_{30}u^3 \quad (3-3)$$

and

$$y = b_{00} + b_{01}v + b_{02}v^2 + b_{03}v^3 + b_{10}u + b_{11}uv + b_{12}uv^2 + b_{20}u^2 + b_{21}u^2v + b_{30}u^3 \quad (3-4)$$

This polynomial expression requires the number of control points to be greater than or equal to $((N+1)2(N+2))/2$. For first (linear), second (quadratic) and third (cubic) order polynomials of this form, the minimum number of control points would be 3, 6 and 10, respectively. The total number of unknown terms is twice this number since we must solve for both x and y . That is, we must solve two surface fitting problems each containing $((N+1)2(N+2))/2$ unknowns. These polynomial forms will be addressed again with respect to their application within the multiquadric algorithm for image registration.

A bi-polynomial formulation found in Kratky (1976) and Hall (1979), where $x=f(u,v)$, $y=g(u,v)$, each containing N^2 terms, or coefficients, is given by:

$$x = \sum_{i=0}^N \sum_{j=0}^N a_{ij} u^i v^j \quad (3-5)$$

and

$$y = \sum_{i=0}^N \sum_{j=0}^N b_{ij} u^i v^j \quad (3-6)$$

where,

$$x = a_{00} + a_{01}v + a_{02}v^2 + a_{03}v^3 + a_{10}u + a_{11}uv + a_{12}uv^2 + a_{13}uv^3 + a_{20}u^2 + a_{21}u^2v + a_{22}u^2v^2 + a_{23}u^2v^3 + a_{30}u^3 + a_{31}u^3v + a_{32}u^3v^2 + a_{33}u^3v^3 \quad (3-7)$$

and

$$y = b_{00} + b_{01}v + b_{02}v^2 + b_{03}v^3 + b_{10}u + b_{11}uv + b_{12}uv^2 + b_{13}uv^3 + b_{20}u^2 + b_{21}u^2v + b_{22}u^2v^2 + b_{23}u^2v^3 + b_{30}u^3 + b_{31}u^3v + b_{32}u^3v^2 + b_{33}u^3v^3 \quad (3-8)$$

The bi-polynomial form is implemented in the data visualization package IDL (Interactive Data Language; 1993). The inclusion of the additional higher order terms increases the ability of the polynomial expression to model complex patterns. However, this formulation provides solutions that differ depending on the location of the origin. An infinite number of surfaces is possible, each one generated by shifting the origin in to any new

arbitrary location. This characteristic, generating an arbitrary surface, may be regarded as undesirable and extends to parameter subset selection procedures such as backward stepwise regression too.

The best polynomial expression used in image warping depends upon the scene geometry. In fact, additional forms are possible by excluding coefficients in either the polynomial or bi-polynomial form. However, this is not common practice in remote sensing. An exception in the literature is Leckie (1980) who does not restrict the polynomial equations as shown above. The caveat to determining which functional form to use is with respect to invariance properties. The conventional polynomial approach is affine invariant under interpolating conditions and invariant with respect to rigid motions for approximation. This is not true for the bi-polynomial formulation or the treatment that was used by Leckie. In these cases, the orientation of the reference coordinate system produces a unique model under most circumstances.

It is interesting to note that the commercial image processing software packages by ERDAS and PCI implement the models with some operational emphasis on identifying “bad” control points. This is useful, but it ignores the fact in airborne scanner imagery, a seemingly bad control point may in fact be indicative of high local variation which will confound the registration process. Deleting the bad point may improve the fit for some areas, but there will be high local distortion in the region where the point was deleted. Greater flexibility in polynomial specification must be regarded as a necessity and not merely a desirable feature. Local polynomial methods may improve upon the results, though it is not clear that the inherent shortcomings of the method warrant the additional computational cost that would be incurred (Goshtasby 1988a).

It should also be apparent that the surface fitting problem is in fact two problems. There is no justification for not using the best polynomial for modeling each of the x and y distortions, even if a different polynomial expression is used for x and y . This is especially applicable to airborne scanners which are roll-stabilized. For example, at high altitude or over flat terrain the across-flight-path distortions may be less than the along-flight-path distortions. In other circumstances the topographic effects may quite large such that the across-flight distortions are greater in magnitude than the along-flight-path distortions.

3.2 Finite Element Methods

In remote sensing, the *finite element method* has come to be synonymous with piecewise linear interpolation over triangles. Image warping via the decomposition of an image into a series of pieces, or surface patches, gives rise to a number of issues specific to local interpolation. This procedure is referred to as a piecewise interpolation; it is a local approach to geometric correction. The pieces are termed finite elements from engineering nomenclature.

The use of finite elements for image warping was first implemented for quadrilaterals using bilinear functions in VICAR/IBIS (Video Image Communication and Retrieval/Image Based Information System; see Appendix) at JPL (Jet Propulsion Laboratory) in 1976 (Zobrist 1994). A description of the use of control grids, hence control points, in VICAR for the construction of these finite elements may be found in Castleman (1979). Between 1976 and 1979, the use of finite elements was expanded to include triangulations of the control points; control points are often referred to as tiepoints and tie points in VICAR. In 1979, the use of triangular finite elements with bilinear functions was being used to mosaic Landsat imagery by EROS Data Center (Zobrist, Bryant and McLeod 1983).

The polynomial functions for the piecewise bilinear registration of sub-intervals (subareas) are presented below. In the first case, we show how a bilinear transformation is applied as an inverse mapping. The rectangles in the base image are mapped to the (distorted) input quadrilaterals such that an input image point per quadrilateral is found using the following expression:

$$x = a_0 + a_1u + a_2v + a_3uv \quad (3-9)$$

and

$$y = b_0 + b_1u + b_2v + b_3uv \quad (3-10)$$

The piecewise solutions to the bilinear transformations are generated from the vertices of the rectangles in the output space. These rectangular patches interpolate at the vertices of a region and approximate the unknown locations within the region over which they are defined. In matrix notation, we solve the following system of equations for each surface patch:

$$\begin{bmatrix} x_0 & y_0 \\ x_1 & y_1 \\ x_2 & y_2 \\ x_3 & y_3 \end{bmatrix} = \begin{bmatrix} u_0 v_0 & u_0 & v_0 & 1 \\ u_1 v_1 & u_1 & v_1 & 1 \\ u_2 v_2 & u_2 & v_2 & 1 \\ u_3 v_3 & u_3 & v_3 & 1 \end{bmatrix} \begin{bmatrix} a_3 & b_3 \\ a_2 & b_2 \\ a_1 & b_1 \\ a_0 & b_0 \end{bmatrix} \quad (3-11)$$

Bilinear transformations offer ease of implementation, but the transformations are not over the smallest definable surface patches. The quadrilaterals may be decomposed into triangles simply by connecting a pair of opposite vertices. The smaller patches improve the model fit in the presence of rapidly varying local distortions. It is only necessary to drop the cross-product (uv) to define a mathematical function over triangles. These functions interpolate through the vertices as in the rectangular case where each input image point is found as follows:

$$x = a_0 + a_1 u + a_2 v \quad (3-12)$$

and

$$y = b_0 + b_1 u + b_2 v \quad (3-13)$$

In matrix notation, a solution for the following system of equations is generated for each finite element by solving this system:

$$\begin{bmatrix} x_0 & y_0 \\ x_1 & y_1 \\ x_2 & y_2 \end{bmatrix} = \begin{bmatrix} u_0 & v_0 & 1 \\ u_1 & v_1 & 1 \\ u_2 & v_2 & 1 \end{bmatrix} \begin{bmatrix} a_2 & b_2 \\ a_1 & b_1 \\ a_0 & b_0 \end{bmatrix} \quad (3-14)$$

The tessellation of an image into pieces requires a triangulation of the control point set. An arbitrary triangulation would suffice, but a more appealing approach is to form triangles based on proximity. We would like to model effectively each subregion of an image. A robust method will generate triangles which are well-shaped, or close to equiangular. This requirement requires nearby points to define the tessellation such that we are more likely to capture and model geometric distortions when using surface patches.

VICAR uses the classic *Greedy triangulation* of the point set. From Manacher and Zobrist (1979) and Zobrist *et al.* (1991) we describe the process of generating a Greedy triangulation for a given point set: (1) considering the $n(n-1)/2$ undirected edges; (2) insert the shortest edges first; and (3) continue until the entire point set is triangulated. Edges are not inserted if they would intersect previously placed lines.

Triangulations in the IBIS successor CAGIS (Cartographic Analysis and Geographic Information System; Rand Corporation) may be generated using the greedy method or the *max-min angle criterion* (maximize the minimum angle for each triangle over all triangulations) or the *circle criterion* (no point is within the circumcircle of any triangle). The latter criteria are equivalent and yield the well-known *Delaunay triangulation* (see Aurenhammer 1985). The Delaunay triangulation has the property whereby the insertion or deletion of a point has only a local effect. That is, a change in the triangulation does not cause a rippling effect throughout the image (Gold 1994). Much has been written about the Delaunay triangulation and its graph-theoretic dual, the Voronoi diagram (see Okabe, Boots, and Sugihara 1992).

There are other criteria for generating spatial tessellations. For example, the *optimal triangulation* is defined in the computational geometry literature as the *minimum length triangulation*. The optimal triangulation minimizes the sum of the edge lengths over all triangulations. This is also known as the

minimum-weight triangulation (Preparata and Shamos, p. 227 1985; from Snoeyink 1994). The computational complexity of finding the minimum-weight triangulation remains an open research question (Snoeyink 1994). Neither the Greedy nor the Delaunay criterion approximate the optimal triangulation (Manacher and Zobrist 1979), but on the average the Delaunay criterion yields triangles which are close to optimal in minimum edge length (Lingas 1986; in Aurenhammer 1985). There is no best triangulation criterion or criteria for modeling image distortions. The best triangulation is dependent upon the nature of the image distortions in the remotely sensed imagery—*i.e.* it is surface or data-dependent.

EROS Data Center's LAMS (Large Area Mosaic System; see Thormodsgard and Lillesand 1987) and Rand Corporation's Cartographic Analysis and Geographic Information System (CAGIS; Zobrist *et al.* 1991) currently have both the Greedy and Delaunay criteria as options for registration, rectification and mosaicking. VICAR software is available through the NASA software depository COSMIC, located at the University of Georgia (See Appendix). VICAR can be easily modified to include different triangulation criteria.

Data-dependent triangulations which are optimal with respect to some criteria are a recent development. These triangulations may result in long skinny triangles which are traditionally avoided for two principal reasons: (1) Numerically, long skinny triangles are more difficult to handle; and (2) Conceptually, long skinny triangles cover greater distances which may preclude effectively modeling of local distortions. Clearly the advantage of data dependent triangulations is that the local distortions may indeed be such that the Delaunay, or close-to-equiangular triangles, and other data-independent triangulations are less than satisfactory for the task. Two recent papers by Dyn and Rippa (1993) and Rippa (1992) are starting points into this literature. See also Schumaker (1993), where simulated annealing is shown to be useful for searching for different triangulation criteria as well as data-dependent triangulations.

Piecewise linear image registration has been periodically reintroduced in the literature. The technique is described by Goshtasby (1986) and Devereux, Fuller, Carter and Parsell (1990). In each case, the piecewise case is developed as an alternative to the polynomial methods described previously. See also Saalfeld (1985), Spiess and Brandenberger (1986), and White and Griffin (1985) for a cartographic perspective.

It is possible to derive higher degree triangular or rectangular elements (see Lawson 1977). For example, Goshtasby (1987) describes the application of cubic functions to the registration problem. Parr and Comer (1990) implemented Akima's quintic method (Akima 1978a, 1978b) in TASCs in-house image processing system DIMS (Digital Image Management System, The Applied Sciences Corporation). Akima's method is also implemented in the IDL software package (Interactive Data Language; 1993). It was noted previously that IDL is principally a visualization package. IDL was unable to handle the large datasets such as those used in this research.

In general usage, Akima's method refers to the article and algorithm published in *ACM Transactions on Mathematical Software* (Association of Computing Machinery; 1978). Akima (1984) introduced a variation of this scheme, specifically changing the computational method for estimating first partial derivatives. Akima's revision was packaged in IMSL as subroutine IQHSCV (International Mathematical and Statistical Library, Edition 8, 1980). Akima (1984) suggests modifications to the ACM and IMSL routines, the former generally providing better results while the latter is computationally faster.

3.3 Radial Basis Functions Methods

Hardy's multiquadric method (1971) belongs to a family of radial basis functions. We limit our discussion to the two methods which have appeared in the literature for image warping: thin plate splines (TPS) and the multiquadric (MQ) method. The focus in this section is on the interpolating characteristics of these functions in their fundamental forms. These methods are global in these sense that all control points are used to construct the basis functions for the surface fitting models.

It is almost certain that the delayed introduction of radial basis functions to image registration is due to the increased computational requirements vis-a-vis the traditional polynomial and finite element methods. There are also some practical issues surrounding the solution procedure which are related to the number of observations. As an aside, radial basis functions have been applied to large data sets where “blending” was

required because of the large number of observations. Specifically, the number of observations exceeded the capability of the solution procedures for a given number of points such that more than one surface fitting model is used to develop the surface. Special techniques are required to merge the multiple surfaces. This suggests that image registration with radial basis functions may be usefully extended to mosaicking or to independently model badly distorted pieces of a larger scene. Shiro and Williams (1984) implement adaptive surface fitting using the MQ method as do Mitsova and Mitas (1993) in segmented processing of terrain data.

Hardy's multiquadric exhibits tension-like effects, or surface smoothing as it is sometimes called with respect to the specification of the multiquadric parameter. Determination of the best multiquadric parameter has been the subject of considerable research (Franke 1979, 1982a; Tarwater 1985; Carlson and Foley 1991; and Carlson and Foley 1992). In a similar, but theoretically different manner, the thin plate spline may also be defined in such a way that local distortions can, to some extent, be controlled for in the distortion model. Franke (1985) describes the concept of tensioning for thin plate splines.

For more information on these methods, we direct the reader to Hardy's review of multiquadric-biharmonic theory and applications and the Special Issue on radial basis functions in *Computers & Mathematics with Applications* (Volume 24, Number 12, 1992). Theoretical discussions which are relevant include Duchon (1976), Meinguet (1979), Micchelli (1986) and Powell (1987). Also, Bookstein (1989) provides a quantitative biology perspective where the problem is one of comparing biological forms as deformations. Tobler (1994) analyzes cartographic distortions in a similar fashion.

3.3.1 Thin Plate Splines

The first application of thin plate splines for surface fitting and image warping discovered during our literature search was by Goshtasby (1988b, 1993). Goshtasby applies the surface splines of Harder and Desmarais (1972) to the warping problem. These surface splines were later called thin plate splines by Duchon (1976) reflecting the nature of the surface fitting problem. The thin plate spline problem may be envisioned as one where a thin flexible plate is being deflected by point loads. The TPS solution minimizes the amount of bending energy applied to the surface. A full treatment of the development and theory of TPS is well beyond the scope of this report. We refer the reader to Franke and Nielson (1991) as a point of entry into the thin plate spline literature.

Recently, Flusser (1992) addressed thin plate splines in an exposition on adaptive image registration techniques. Flusser's paper referenced earlier work on the TPS by Goshtasby (1988b). Goshtasby (1988b) presented the surface spline formulation of Harder and Desmarais as opposed to the TPS formulation commonly found in the literature. Equivalent surfaces result despite the differences in the problem formulation. Barrodale, Kurahawa, Pockert and Skea (1993) implement the thin plate spline for sonar-scanned data. Barrodale, Skea, Berkley, Kuwahara and Poekert (1993) commented on Flusser's work using the TPS formulation. Barrodale *et al.* note that recent algorithmic developments by Powell (1992) reduce the computational complexity of image registration by TPS making its application more feasible. Barrodale *et al.* have implemented Powell's procedure realizing improvements of around two orders of magnitude depending on the number of control points.

We present Harder and Desmarais' surface spline and the TPS formulations below. Our purpose is to illustrate that the same surface results from either formulation, although certain coefficients in the solution may be different. Our notation emphasizes the application of TPS to image warping. The surface spline as described by Goshtasby (1988b) and Flusser (1992) is shown below for $x=F(u,v)$ and $y=G(u,v)$:

$$F(u,v) = a_0 + a_1u + a_2v + \sum_{i=1}^N f_i r_i^2 \ln r_i^2 \quad (3-15)$$

and

$$G(u, v) = b_0 + b_1 u + b_2 v + \sum_{i=1}^N g_i r_i^2 \ln r_i^2 \quad (3-16)$$

The latter terms, *i.e.* the summations, are written out below for clarity:

$$\sum_{i=1}^N f_i r_i^2 \ln r_i^2 = \sum_{i=1}^N f_i \left(\sqrt{(x-x_i)^2 + (y-y_i)^2} \right)^2 \ln \left(\sqrt{(x-x_i)^2 + (y-y_i)^2} \right)^2 \quad (3-17)$$

and

$$\sum_{i=1}^N g_i r_i^2 \ln r_i^2 = \sum_{i=1}^N g_i \left(\sqrt{(x-x_i)^2 + (y-y_i)^2} \right)^2 \ln \left(\sqrt{(x-x_i)^2 + (y-y_i)^2} \right)^2 \quad (3-18)$$

The following “equilibrium constraints” are imposed:

$$\sum_{i=1}^N f_i = \sum_{i=1}^N f_i u_i = \sum_{i=1}^N f_i v_i = 0 \quad (3-19)$$

and

$$\sum_{i=1}^N g_i = \sum_{i=1}^N g_i u_i = \sum_{i=1}^N g_i v_i = 0 \quad (3-20)$$

where, N = the number of control points and r^2 is defined as:

$$r_i^2 = \left[r_i(u, v) \right]^2 = (u - u_i)^2 + (v - v_i)^2 \quad (3-21)$$

This is simply the distance squared from control point i to all other control points. The TPS formulation of Barrodale *et al.* is given below:

$$F(u, v) = a_0 + a_1 u + a_2 v + \sum_{i=1}^N f_i r_i^2 \ln r_i^2 \quad (3-22)$$

and

$$G(u, v) = b_0 + b_1 u + b_2 v + \sum_{i=1}^N g_i r_i^2 \ln r_i^2 \quad (3-23)$$

The difference in the basis functions is with respect to the inclusion of a constant in the surface spline formulation which is not necessary for the solution of the problem. Note the following equivalence:

$$r^2 \ln r^2 = 2 \cdot r^2 \ln r \quad (3-24)$$

Clearly, the former expression is computationally less intensive, *i.e.* one less square root operation. It will be helpful at this time to construct the system of equations which must be solved for the image warping problem for N control points, $N=1, 2, \dots, n$:

$$\begin{bmatrix}
0 & 0 & 0 & 1 & 1 & \dots & 1 \\
0 & 0 & 0 & u_1 & u_2 & \dots & u_n \\
0 & 0 & 0 & v_1 & v_2 & \dots & v_n \\
1 & u_1 & v_1 & 0 & r_{12}^2 \ln r_{12} & \dots & r_{1n}^2 \ln r_{1n} \\
1 & u_2 & v_2 & r_{21}^2 \ln r_{21} & 0 & \dots & r_{2n}^2 \ln r_{2n} \\
\dots & \dots & \dots & \dots & \dots & \dots & \dots \\
1 & u_n & v_n & r_{n1}^2 \ln r_{n1} & r_{n2}^2 \ln r_{n2} & \dots & 0
\end{bmatrix}
\begin{bmatrix}
a_0 & b_0 \\
a_1 & b_1 \\
a_2 & b_2 \\
f_1 & g_1 \\
f_2 & g_2 \\
\dots & \dots \\
f_n & g_n
\end{bmatrix}
=
\begin{bmatrix}
0 & 0 \\
0 & 0 \\
0 & 0 \\
x_1 & y_1 \\
x_2 & y_2 \\
\dots & \dots \\
x_n & y_n
\end{bmatrix} \quad (3-25)$$

where $r_{ij} = r_i(u_j, v_j)$, or the distance from control point (u_i, v_i) to control points (u_j, v_j) for all i and j ($i, j=1, 2, \dots, n$).

Characteristics and solution procedures for these equations are discussed in Barrodale *et al.* The inclusion of a first order polynomial in this system is of fundamental interest. These terms, the equilibrium conditions, result in a surface which, “grows almost linearly when far away from the points (x_j, y_j) ” (Barrodale *et al.*). The TPS implicitly, *i.e.* by definition, includes polynomial precision of degree one.

During a review of scattered data contouring, Sabin (1980) reports that the kernel in the basis may be replaced with r^3 which yields a function behaving in a similar manner and potentially more useful when extrapolation is an issue. This shall be investigated in the near future.

It is unclear in the implementation by Barrodale *et al.* whether they are modeling the distortion based on a preliminary fit using a polynomial expression or the control points alone. For both the TPS and MQ method, it is feasible to model the residuals based on a preliminary polynomial fit. That is, a preliminary approximation, or interpolation orienting the images and removing some distortion may improve the quality of the final warp. Barrodale *et al.* may assume that for their application, the registration of sidescan sonar imagery, that the images are oriented in the same direction with nominal distortions, hence there is no need for polynomial preprocessing. We note that preprocessing creates a new set of surface fitting problems (one for x and one for y).

We conjecture that in the affine (first order) case, the thin plate spline should produce the same or similar solution. The thin plate spline is a minimum curvature technique and an affine transformation will change the relative locations of the control points, though not introducing additional “curvature” as with higher order polynomials. Clearly, the best preliminary fit will be one where the input control points are distributed in a pattern similar, if not identical, to the output control points. Further comments on this subject are found in the next section.

Preliminary fitting functions do not jeopardize the radiometric fidelity of the remotely sensed data. On the contrary, by improving the geometric distortion model, we retain data quality for applications such as change detection and multi-temporal classification. Multi-stage geometric processing does not imply multiple resampling. Only a single resampling is required to perform digital warping.

3.3.2 Hardy's Multiquadric Functions

The development of the surface spline and multiquadric functions occurred at approximately the same time. Hardy's multiquadric was first published in 1971, while Harder and Desmarais' surface spline was published as an “Engineering Note” in 1972. It was later discovered that the two methods have much in common. Hardy's multiquadric takes two general forms: the multiquadric method (MQ) and the reciprocal multiquadric method (RMQ). Our discussion will focus on the MQ method. For completeness, the formulations for both methods are given below. However little further mention will be given to the RMQ.

The literature on the multiquadric method is vast. We are fortunate that Hardy published a retrospective in 1990. In this multiquadric review, Hardy refers to this technique as the multiquadric-biharmonic method. He also lists over 100 references to the MQ many of which are relevant to remote

sensing. We are selective in our coverage of this literature, and emphasize the practical issues most closely related to the scope of this project. We note that the solution to the multiquadric system of equations is not always biharmonic and will continue to use the expression “multiquadric method” (Franke 1994).

The potential for image or cartographic warping using the MQ is alluded to by Hardy in *Photogrammetric Engineering and Remote Sensing* in 1977. No precise details were given on the application. The multiquadric image warping implementation detailed here is described by Göpfert (1982). Ehlers (1987) recognized the potential of Göpfert's multiquadric formulation for image warping and supervised its implementation by Flottemesch (1993). This effort was supported as part of this research and resulted in the development of research software.

In the sense of polynomial precision, as the term is used in the scattered data interpolation literature (e.g., Franke and Nielson 1991), the original MQ includes no polynomial precision. However, it may be appropriate, operationally, to include polynomial precision in the manner described for thin plate splines. Franke (1987) and Franke and Nielson (1991) describe subsequent developments by Micchelli (1986) where it is noted that there is always a solution to the MQ basis. However, with respect to Hilbert Space Theory, a constant term should be included to derive a solution for the MQ method. This is in contrast to the TPS where a constant, an x -term and a y -term are specified.

Based on the definitions above, we develop our distortion model for $x=F(u,v)$ and $y=G(u,v)$ based on the MQ kernel:

$$F(u,v) = \sum_{i=1}^N f_i \sqrt{(x-x_i)^2 + (y-y_i)^2 + R^2} \quad (3-26)$$

and

$$G(u,v) = \sum_{i=1}^N g_i \sqrt{(x-x_i)^2 + (y-y_i)^2 + R^2} \quad (3-27)$$

The RMQ functions are similar:

$$F(u,v) = \sum_{i=1}^N f_i \frac{1}{\sqrt{(x-x_i)^2 + (y-y_i)^2 + R^2}} \quad (3-28)$$

and

$$G(u,v) = \sum_{i=1}^N g_i \frac{1}{\sqrt{(x-x_i)^2 + (y-y_i)^2 + R^2}} \quad (3-29)$$

The remainder of this section refers to the MQ formulation. We make some observations regarding the RMQ in the following section where we review some experimental results. This cautious approach reflects the relatively poor performance of the RMQ for geometric correction which is unlike its performance in conventional applications given (x,y,z) data.

The MQ basis functions are often more concisely expressed as:

$$F(u,v) = \sum_{i=1}^N f_i \sqrt{(r_i^2) + R^2} \quad (3-30)$$

and

$$G(u, v) = \sum_{i=1}^N g_i \sqrt{(r_i^2) + R^2} \quad (3-31)$$

The similarity between this expression and the lower right partition of the TPS matrix should not go unnoticed. The solution to this problem is generated from the following system of equations:

$$\begin{bmatrix} 0 & 1 & 1 & \dots & 1 \\ 1 & \sqrt{r_{11}^2 + R^2} & \sqrt{r_{12}^2 + R^2} & \dots & \sqrt{r_{1n}^2 + R^2} \\ 1 & \sqrt{r_{21}^2 + R^2} & \sqrt{r_{22}^2 + R^2} & \dots & \sqrt{r_{2n}^2 + R^2} \\ \dots & \dots & \dots & \dots & \dots \\ 1 & \sqrt{r_{n1}^2 + R^2} & \sqrt{r_{n2}^2 + R^2} & \dots & \sqrt{r_{nm}^2 + R^2} \end{bmatrix} \begin{bmatrix} a_0 & b_0 \\ f_1 & g_1 \\ f_2 & g_2 \\ \dots & \dots \\ f_n & g_n \end{bmatrix} = \begin{bmatrix} 0 & 0 \\ x_1 & y_1 \\ x_2 & y_2 \\ \dots & \dots \\ x_n & y_n \end{bmatrix} \quad (3-32)$$

The best value for the parameter R^2 is determined by both the relative distances of the control points as well as the magnitude of the (x,y) distortions. In Göpfert's algorithm, we model the residuals generated from a preliminary polynomial function. As noted in the section on thin plate splines, it also generates an (x,y) surface where the control points are distributed much like in the (u,v) plane.

Göpfert's algorithm is composed of four principal steps:

- [1] Model the global geometric distortion of the $(x,y) = f(u,v)$ using a bivariate mapping polynomial expression. This is an inverse transformation intended to remove the global trend in the data.

$$[x, y]^P = [P_x(u, v, x), P_y(u, v, y)]$$

- [2] Find the residual distortion (actual - predicted) from [1].

$$(x^r, y^r) = [x, y]^R = [[x, y] - [x, y]^P]$$

- [3] Model the residual distortion (not to be confused with error) from [2] using the MQ method. That is, model the distortion as $(x^r, y^r) = f(u,v)$.

$$[x, y]^{MQ} = [MQ_x(u, v, x^r), MQ_y(u, v, y^r)]$$

- [4] Add the predicted values from [1] and the MQ values from [3] to generate (x,y) as a function of (u,v) .

$$(x, y) = [x, y] = [x, y]^P + [x, y]^{MQ}$$

In Step #1 we are confronted with the dilemma of what constitutes the best polynomial for the distortions per the dataset. In Step #2 we must choose an appropriate value for R^2 . MQE (Multiquadrische Entzerrung), ISPA's multiquadric method software implementation, allows for experimentation with different order polynomials and different values for R^2 . The respective equations for (x,y) are presented below. The values from Step #1 are shown as $P(x)$ and $P(y)$ where P is a polynomial of an arbitrary order:

$$x = P(x) + \sum_{i=1}^N f_i \sqrt{(r_i^2) + R^2} \quad (3-33)$$

and

$$y = P(y) + \sum_{i=1}^N g_i \sqrt{(r_i^2) + R^2} \quad (3-34)$$

In general, the determination of the optimal value for R^2 depends upon the nature of the scene distortions and the number and distribution of control points. In other words, it is problem-dependent. The value of R^2 determines whether the interpolating surfaces will be degenerate conics ($R^2 = 0$) or hyperboloids (Hardy 1990). In the case of (x,y,z) data, there are numerous published methods for generating an appropriate value for R^2 . These do not appear to be directly applicable to image warping. Our experience shows that data spacing may be more important or rather the spacing and adequate sampling of the distortions.

3.3.2.1 R^2 and (X,Y,Z) Data

Despite the fact that previous work on finding optimal values using heuristics for R^2 does not directly apply to the warping problem, it is appropriate to review previous work. This provides us with a starting point for further investigations. We discuss research on finding a good value for R^2 in some detail since the quality of the interpolating functions depends on this value. Hardy (1977) recommended the following equation for R^2 :

$$R^2 = 0.665 \cdot d^2 \text{ or } R = 0.815 \cdot d \quad , \quad (3-35)$$

where d is the “grid spacing of the nodes.” Clearly, when the data are irregularly spaced this must be re-interpreted. Franke (1979) notes that d is approximately the mean distance to its nearest neighbor. Franke (1979) introduced an alternative to this equation:

$$R^2 = \left[\frac{NPPR}{10} \cdot \frac{1}{2} \left(\frac{D}{\sqrt{n}} \right) \right]^2 \text{ or } R^2 = \left[\frac{NPPR}{10} \cdot \frac{r}{\sqrt{n}} \right]^2 \quad (3-36)$$

where $NPPR$ is a weighting parameter, D is the diameter of the bounding point set (or r is the radius) and n is the number of data points. (The meaning of the abbreviation for the $NPPR$ weighting parameter (Number of Points per Region) is irrelevant for the MQ method. It is simply a variable name used in Franke's (1979) surface fitting simulations by Franke (1994). $NPPR$ was set to 25 by Franke who noted that higher values on occasion produced promising results. This formula appears most often in the scattered data interpolation literature (*e.g.* Carlson and Foley 1991 and Wolberg 1990) as:

$$R^2 = \left[1.25 \cdot \frac{D}{\sqrt{n}} \right]^2 \text{ or } R = 1.25 \cdot \frac{D}{\sqrt{n}} \quad (3-37)$$

where r “is the radius of the disk which could be anticipated to contain one point,” thus $NPPR$ is 25 (Franke 1979). Simplifying Franke's formulation, Foley (1987) approximates the average bounding circle using an average bounding rectangle:

$$R^2 = \left[4.0 \cdot \frac{A}{n} \right]^2 \quad (3-38)$$

where A is the area of the bounding rectangle $((\max(x)-\min(x)) \cdot (\max(y)-\min(y)))$. Subsequently, Carlson and Foley (1991) presented an algorithm for determining an effective MQ parameter. This latter algorithm reportedly yields a value which gives good results and is more robust than the aforementioned methods. Carlson and Foley (1991) report that the magnitude of the z -values is significant in determining an optimal value for R^2 which is counter to most previous research which focused on the distances between the scattered data values. We did not apply this heuristic to our warping problem.

Hardy (p. 188, 1990) cites a formula by Schul'min and Mitel'man (1974) used in a topographical mapping application. Schul'min and Mitel'man's solution may find application to image warping in a modified version presented in the next section. In the present case, it is formulated as:

$$R^2 = \frac{\sum_{i=1}^n \sum_{j=1}^n \left[(x_i - x_j)^2 + (y_i - y_j)^2 \right]}{n(n-1)} \quad (3-39)$$

We expect that the nature of warping remotely sensed data will require the development of new heuristics for approximating the best multiquadric parameter. In limited testing, no one method appeared best for geometric correction. Carlson and Foley provide a heuristic that requires scaling the data to $[0,1]^3$ $((u,v,x)$ and $(u,v,y))$. As a side effect, scaling improves the quality of the solution with respect to numerical accuracy.

3.3.2.2 R^2 and (U,V,X,Y) Data

The determination of the best multiquadric parameter R^2 for the image warping implementation by Flottesch (1993) loosely follows Göpfert (1982). Both formulations are shown below. Note that the difference between the two is with respect to calibrating the MQ parameter based on either the input space (x,y) or the output space (u,v) . Both methods require finding the minimum spacing between data points and multiply this by the constant 0.6. Flottesch writes in his thesis (1993; p. 37):

$$G = R^2 = 0.6 \cdot \min \left(\sqrt{(x_i - x_j)^2 + (y_i - y_j)^2} \right) \quad (3-40)$$

This is not strictly in conformance with Göpfert (1982). Indeed, it seems more appropriate to base the calculation of an optimal R^2 on the spacing of the (u,v) points, especially if a rectified image constitutes the output space. Göpfert's (1982) implementation by Flottesch should therefore be given as:

$$G = R^2 = 0.6 \cdot \min \left(\sqrt{(u_i - u_j)^2 + (v_i - v_j)^2} \right) \quad (3-41)$$

Interestingly, in Göpfert (1977 and 1982), the formulation is given differently. Based on these papers, the following equivalent formulation is given:

$$G = R^2 = 0.6 \min \left((u_i - u_j)^2 + (v_i - v_j)^2 \right) \quad (3-42)$$

The final method we will present here is an adaptation of Schul'min and Mitel'man (1974) where we sum over the distances between (u,v) data points instead of squared data points. This change was based on the observation that the R^2 value would be quite similar to that of Göpfert (1977):

$$R^2 = \frac{\sum_{i=1}^n \sum_{j=1}^n \sqrt{(x_i - x_j)^2 + (y_i - y_j)^2}}{n(n-1)} \quad (3-43)$$

Again, the approximation or determination of the optimal R^2 will be scene (and application) dependent and remains an open research question. The set of possible values for R^2 may be data dependent, or specified for each point as well. That is to say, we are not limited to a single value for each basis functions. There can be as many R^2 values as data points. We clarify this statement below.

Tarwater (1985) mentions the possibility of using a unique R^2 for each data point. This scheme may more effectively account for variable sparse or dense data patterns as well as better model rapidly changing data values. From Carlson and Foley (1991), we can rewrite the basis functions as:

$$x = P(x) + \sum_{i=1}^N f_i \sqrt{(r_i^2) + R_i^2} \quad (3-44)$$

and

$$y = P(y) + \sum_{i=1}^N g_i \sqrt{(r_i^2) + R_i^2} \quad (3-45)$$

This strategy may or may not improve the fit of the interpolating surface (Carlson and Foley 1991), but does illustrate the flexibility of the multiquadric method. Kansa (1990a and 1990b) uses a flexible value for R^2 , however, as noted by Carlson and Foley (1991), the motivation is to improve the condition number of the basis function. Franke, Hagen and Nielson (1994) indicate that it is quite easy to find examples where different multiquadric parameter values lead to singular systems.

3.4 Radial Basis Functions and Polynomial (Functional) Precision

The concept of *polynomial precision* has been introduced here without explanation. For this report, it may be defined as the inclusion of terms in the basis which will reproduce *exactly* a polynomial surface of the same precision given an absence of error in the control points. If there is error, then the polynomial precision may be thought of as a *functional precision* weighted by the kernel. Details on this may be found in Lancaster and Salkauskas (1986, p. 263) for thin plate splines.

The inclusion of polynomial precision is relevant given recent publications by Ruprecht and Müller (1993; 1995), Arad, Dyn, Reinfeld and Yeshurin (1994) and Ruprecht, Nagel and Müller (1995) as it applies to the multiquadric method. The applications described in these publications include linear precision in the basis. Polynomial precision may improve the fit away from the control points, but for remote sensing applications this formulation demands further study. As a counter-example, Franke (1987) reports his experience that the inclusion of a constant reduces the effectiveness of the multiquadric method. Further application-specific research is warranted. Our own limited set of experiences is such that the inclusion of linear precision reduces the overall quality of the warp as determined by the RMSE.

Related to the mathematical formulation of radial basis functions, it is appropriate to note stochastic methods in geostatistics have shown a relationship between thin plate splines and universal kriging (see Cressie (1989), and Wahba (1990) and Cressie (1990)). In meteorology, Nuss and Titley (1994; see "Comments" by Barnes 1995) recently applied the multiquadric method to objective analysis. They included smoothing, in the statistical sense, in their discussion. We will focus on non-stochastic methods while recognizing a related literature exists meriting further investigation do to similarities in mathematical structure. Mitasova and Mitas (1993) describe still another radial basis function (with constant precision).

4 Las Vegas Experiment

The evaluation of the multiquadric method for image registration is carried out over one scene. The scene is conspicuously flat and distorted more in the across-flight line direction. The need for additional comparisons, such as for the case of satellite imagery or rapidly varying topography was lessened as it became clear that the multiquadric method was performing extremely well. Subsequently, the focus of the project shifted to fully documenting the nature and characteristics of the multiquadric method.

This section provides a description of the test site, an overview of the computing environment and a comparison of the results from the three different methods (polynomial, finite element and multiquadric). At the end of the section, we review the MQE software and make recommendations on those issues surrounding the operational implementation of the multiquadric method.

4.1 Test Images

The Las Vegas image set consists of a digitized aerial photograph and an airborne scanner acquired image of the Remote Sensing Laboratory complex on Nellis Air Force Base, Nevada. The reference, or base image in this experiment is a digitized photograph acquired using a Hasselblad 70mm camera. The distorted image was acquired from an airborne multispectral scanner (Daedalus AADS1268) being flown from a BO-105 helicopter platform. The Daedalus scanner imagery includes high frequency distortions induced from platform motion during the scanning procedure.

The Daedalus scanner includes built-in roll correction mechanisms for perturbation from the normal flight line. However, variations in pitch, yaw, altitude and velocity are not compensated for and introduce geometric distortions in the imagery. The vertical aerial photograph has a nominal digitized resolution of approximately one foot per pixel. The scanner imagery is one-third the spatial resolution of the photograph (three feet per pixel).

Control points were collected by ISPA. A scan-digitized image of the base photograph was used to aid in the collection of control points. A Sharp JPX-600 Color Scanner was used at a resolution of 300 dots per inch. The control points are distributed throughout the scene area of interest, though not in a uniform manner. The lack of identifiable features constrained the selection of control points to specific areas. This problem is often encountered when registering multispectral scanner imagery. A subset of the control points were extracted and subsequently used as independent check points. These have a similar, approximately uniform, distribution.

The distorted and reference images are shown in the *Las Vegas Images Appendix*. The following Appendix, *Control and Check Points*, includes two reference images showing the distribution of the control

points and the check points, respectively. The locations of the control and check points are approximate in these graphics based on limitations of the plotting software. The tables in the same Appendix present the actual values. The control and check points are based on an origin defined as the center of the upper left pixel that is located in the upper left corner.

4.2 Computing Environment

The computing resources used are briefly described. This includes hardware and software in varying degrees of detail with respect to vendor specifics and version information.

4.2.1 Hardware

The digital image transformations in this experiment were done on a Sun Microsystems IPX running SunOS 4.1.3. During the initial report preparation, checking numerical computations was done using an IBM-compatible 386-25 running MS-DOS 5.0 with a math coprocessor. Subsequent development took place on the IPX platform and on an IBM-compatible Pentium-90 processor (without the notorious floating point hardware bug). The MQ software, in its various manifestations, has been tested and used to check the results on an SGI-Indigo2-XZ.

4.2.2 General Purpose Software

On the 386-25 computer, Borland's Quattro Pro spreadsheet, Version 2.0, was used to double-check such things as RMSE (Root Mean Squared Error) calculations and calculation of image extents by ERDAS and MQE. Additional checks were made using Statistical Sciences S-Plus Version 3.1 and 3.2. S-Plus was also used to evaluate the polynomial results, Hardy's multiquadric and thin plate splines.

4.2.3 Image Processing and G.I.S. Software

Commercial image processing software, ERDAS, was used for the polynomial registration evaluation. CAGIS was used to evaluate the finite element method. ISPA provided the MQE code for the multiquadric method. Software characteristics are reviewed in the next three sections.

4.2.3.1 ERDAS

The ERDAS software versions used during this project are listed below. There are two separate routines for image warping in ERDAS 7.5: LRECTIFY and NRECTIFY. Both routines require the polynomial coefficients generated from a separate program COORDN. During preliminary investigations, NRECTIFY was used since it duplicates the functionality of LRECTIFY (affine transformation) and has extended capabilities for higher order polynomials. A newer ERDAS system, IMAGINE 8.1, was used as an additional means of validating the results. Below, the version information for the ERDAS software is listed:

- ERDAS 7.5

COORDN -- Coordinate Transformation Version 7.5.04.202
Copyright (C) 1984-1991 Erdas, Inc. All Rights Reserved.
Installation : Remote Sensing Research Unit - UCSB (9/19/91)

- ERDAS 7.5

NRECTIFY -- Non-Linear Rectification Version 7.5.02.202
Copyright (C) 1984-1991 Erdas, Inc. All Rights Reserved.
Installation : Remote Sensing Research Unit - UCSB (9/19/91)

- ERDAS IMAGINE 8.01

Copyright 1991 - 1993 by ERDAS. Inc. All Rights Reserved.

- ERDAS IMAGINE 8.1 Initial Release

Copyright 1991 - 1993 by ERDAS. Inc. All Rights Reserved.
Installation : Remote Sensing Research Unit - UCSB (12/16/93)

The suite of ERDAS registration routines produced consistent results for the geometric modeling component. The nearest neighbor resampled images differed very slightly between the output images attributable to a difference in algorithms in the two products (Kloer 1994).

4.2.3.2 CAGIS

CAGIS (*Cartographic Analysis and Geographic Information System*) was developed at Rand Corporation (Zobrist, *et al.* 1991) and has been provided to the RSRU for use on research projects. CAGIS includes the finite element approach introduced at JPL with VICAR/IBIS. We will describe the registration procedure in CAGIS below:

1. The control points (tiepoints) in the output space are triangulated using either a Greedy triangulation or a Delaunay triangulation.
2. A uniform grid is applied over the output (u,v) space.
3. A warped grid is calculated over the input space by linear interpolation within corresponding triangles.
4. An inverse transformation is used to warp the input image.

There is a built-in function in CAGIS to extrapolate beyond the convex hull of control points. An affine fit by least squares is used to predict the location of four distant points based on the extent of the control points. For more information, see Thormodsgard and Lillesand (1987). The extrapolation, while appropriate for satellite data, does not adequately model distortion outside of the control points. This may not be a problem for environmental modeling using airborne scanners since it is common practice to over fly an area. That is, the area of interest is framed by a buffer. This area outside the region of interest need not be accurately registered.

The gridding step in CAGIS introduces additional error into the registration process. The total registration error includes both the original error from the distortion model and introduced gridding error. In the case of badly warped imagery, the grid spacing in either or both the x and y directions may approach the size of the output image. This would effectively eliminate the error introduced by gridding. The Delaunay and Greedy Triangulations are shown with and without the grid point overlay in the *Triangulations* Appendix. Further reading on the use of gridding techniques in image warping may be found in Niblack (1986) and Wolberg (1990).

The tessellations of the control points in the *Triangulations* Appendix do not appear to be composed entirely of triangular elements. In some cases it appears that there are triangle vertices in the middle of adjacent triangle edges. This is due to the presence of extremely skinny triangles. In fact, the triangulations were verified both quantitatively and visually. In the case of the Delaunay Triangulation, by dropping the four extreme points used to extrapolate in CAGIS, we found the number of triangles to be equal to twice the number of points plus the number of boundary edges less two, or 152. This formula for the number of triangles may be found in Schumaker (1987). This was also the same number of triangles yielded by program VORONOI (Fortune, 1987). The same procedure was followed for the Greedy Triangulation. The number of triangular elements, excluding the extreme points, was also 152. A detailed visual inspection of the plots confirmed these findings.

During the course of the investigation, the Delaunay triangulation (or Thiessen option in CAGIS) was discovered to produce an erroneous tessellation in the output space. The problem was reported to Rand and immediately fixed. As noted previously, this warping software is used by Rand, UCSB, EDC (EROS (Earth Resources Observation Systems) Data Center and Ft. Leavenworth TRAC (TRADOC Analysis Command; TRADOC: Training and Doctrine Command; Zobrist, 1994). The MQ method performed much better in the test case using the Greedy triangulation, such that we did not view this as detrimental to the project. That is,

we anticipated that some improvement was possible with the Delaunay algorithm, but not so much as to change our conclusions. Later, the Delaunay triangulation was used and did indeed yield better results.

CAGIS is flexible in terms of image origins. The orientation of the coordinate system is accommodated for in the specific programs we used, namely TIEGRID and IMWARP. The principal *caveat*, if you will, in using CAGIS with ERDAS 7.5, ERDAS Imagine and MQE is with respect to the coordinates of the image origin. In CAGIS, the origin of the coordinate system (0,0) is such that the center of the pixel at the origin is (0.5,0.5). This contrasts with ERDAS 7.5 and MQE (1,1) and ERDAS IMAGINE (0,0).

4.2.3.3 MQE

MQE (*Multiquadratische Entzerrung*; Multiquadric Rectification) is the name of the software prepared at ISPA under the cooperative research contract between the RSRU and ISPA supporting this research. The source code level used in the 1994 report was version 1.15. RSRU has since enhanced the code during the course of the research (Fogel, 1994 and 1995). The results in this revised report are based on the modified code. The compilers used in the project depended largely on the platform, but in general recent GNU Project C compilers and libraries were used to compile the MQE code (2.6.x).

The relevant characteristics of the image registration/rectification software for the research are listed below:

- ANSI C Language source code
- Compatibility with ERDAS 7.5 *.lan files
- Polynomial order to degree ten
- Input coordinates are based on an upper left origin
- Output coordinates are based on a lower left origin
- Supports polynomial or multiquadric registration method
- Manual selection of the MQ smoothing factor R^2
- Testing routines for evaluating alternative surface fitting models
- A flexible evaluation of the polynomial order as well as the MQ parameter, R^2 , based on a set of control points and check points.
- Nearest neighbor, bilinear interpolation or cubic convolution resampling
- No polynomial precision in the basis

The matrix technique used for all of the problem-solving in this report were based on those described in Golub and Van Loan (1989) and implemented in the matrix library *Meschach* (Stewart and Leyk 1994). Specifically, the QR factorization routine was used. Double-precision results on the workstations were checked against “long” double precision on the PC using Borland C++ 3.1 (using C code).

The MQE has specific requirements related its use for image-to-image or image-to-map registration. Control points must be specified in ERDAS 7.5 format, *i.e.* as a *.gcp file in ERDAS. The origin of the output space is inflexible. This requires that the control points be offset by some number greater than or equal to the number of lines in the scene to perform image-to-image registration. This is the approach the RSRU took in the software evaluation.

There are additional features in MQE which will not be described here. Interest readers are referred to the programmer's thesis (Flottesmesch 1993). For example, in *Menu-Resampling*, it may be necessary to modify the *.lan header to reflect a nominal XCELL,YCELL pixel size to exercise all MQE options. These features are not directly related to the task of registration method comparison, hence they are ignored for this discussion.

The MQE program includes diagnostic output to help identify outliers in the tiepoint set. These diagnostics are not generally applicable to this evaluation task, since we are focusing on the use of these techniques for badly warped imagery.

Göpfert's (1982, pp. 14-16) approximation for the optimal smoothing parameter is given below:

$$R^2 = 0.6 \cdot \min\left(\left(u_i - u_j\right)^2 + \left(v_i - v_j\right)^2\right) \quad (4.1)$$

The use of (u, v) in Equation 4-1 refers to the output space. Flottesmesch (1993) implemented Göpfert's formula allowing a flexible specification following the form indicated in Equations 3-26, 3-27 and 3-28). The MQE program implementation differed from the formulation given in his thesis. The implementation of the smoothing value for the latest version of the code is as follows:

$$R^2 = G \cdot \min\left(\left(u_i - u_j\right)^2 + \left(v_i - v_j\right)^2\right) \quad (4.2)$$

where G is user-specified. We refer to the smoothing factor (Glaettungsfaktor) as Göpfert's G for no other reason than the fact that we are not privy to his earlier work from which the value 0.6 was derived. The value for the multiquadric parameter may differ substantially from the approaches taken by Hardy (1977), Franke (1979) and Carlson and Foley (1991). These approaches use an average distance whereas Göpfert uses the minimum distance.

4.3 Quantitative Results

The results of the three registration methods evaluated in this study are presented below. The accuracy of the registration is evaluated using the root mean squared error. The formulas for the RMSE calculations are straightforward. These are presented below:

$$RMSE_x = \sqrt{\frac{1}{n} \sum_{i=1}^n (x_i - x'_i)^2}, \quad (4.3)$$

$$RMSE_y = \sqrt{\frac{1}{n} \sum_{i=1}^n (y_i - y'_i)^2} \quad (4.4)$$

and

$$RMSE_{total} = \sqrt{\frac{1}{n} \sum_{i=1}^n \left[(x_i - x'_i)^2 + (y_i - y'_i)^2 \right]} \quad (4.5)$$

where n is the number of control points or check points. The finite element and multiquadric methods interpolate the control point locations, hence there are no residuals for the control points. The polynomial method only interpolates the data if the number of control points is the same as the number of unknowns in the polynomial expression. This situation is highly unusual for remotely sensed aircraft data. ERDAS uses the expression above. PCIs EASI/PACE takes a different approach. PCI adjusts for the degrees of freedom of a given polynomial order. This adjustment is presented below:

$$RMSE_x = \sqrt{\frac{1}{n-k} \sum_{i=1}^n (x_i - x'_i)^2} \quad (4.6)$$

$$RMSE_y = \sqrt{\frac{1}{n-k} \sum_{i=1}^n (y_i - y'_i)^2} \quad (4.7)$$

and

$$RMSE_{total} = \sqrt{\frac{1}{n-k} \sum_{i=1}^n [(x_i - x'_i)^2 + (y_i - y'_i)^2]} \quad (4.8)$$

where k is the polynomial order. We fell this is an ill-advised approach for the simple reason that no assumptions are made about the underlying structure of the distortions. At the same time, it can be argued that the true locations of the control points are unknown such that this problem may be viewed as a statistical problem. We have opted to make no such assumptions and view the image warping problem as a deterministic process. Consequently, we have no interest in making judgements on the functional relationships between the output coordinates as they relate to either x or y in the input space. For this report, it is assumed that there is no error in the locational coordinates of (x,y) and (u,v) .

The complicated distortion patterns found in the Las Vegas image are displayed in Figure 4-1. The Figure shows the results from a least-squares affine fit of the reference image to the input image (an inverse transformation). The figure shows the magnitude and direction of the displacements after correction for rotation and translation of the origin and skewing in the x and y directions. The arrows are pointing to the predicted locations of the control points in the warped image based on an affine transformation.

4.3.1 Polynomial Results

The first two tables show the results from the polynomial methods. In each case, three numbers are reported: (1) x -RMSE; (2) y -RMSE; and (3) the *total*-RMSE. Two comments are appropriate. First, the improvement in the x and y directions is not uniform. This reflects the fact that we are independently calculating the x and y distortion models. Unfortunately, there are no existing commercial software packages which we are aware of that offer the flexibility to choose different polynomial orders for x and y . Second, the total RMSE continues to drop for the control points but the check points illustrate the polynomial method's fundamental shortcoming--it is unconstrained between the control points and given to (sometimes) undesirable fluctuations.

On a similar note, there exists no commercial software which allows control over which polynomial terms should be included in the surface fitting model for determining the best model. Ironically, given the lack of progress in this area, this proves to be a good thing. These polynomials are affine invariant. The inclusion or exclusion of different terms to this form of polynomial series may compromise the fact that it is translation, rotation and scale invariant (Franke and Nielson, 1991). Invariant properties of scattered data interpolation methods are discussed in Nielson (1987), Nielson and Foley (1989) and Nielson (1993). As a simple example, different warps may result depending on the origin of the images.

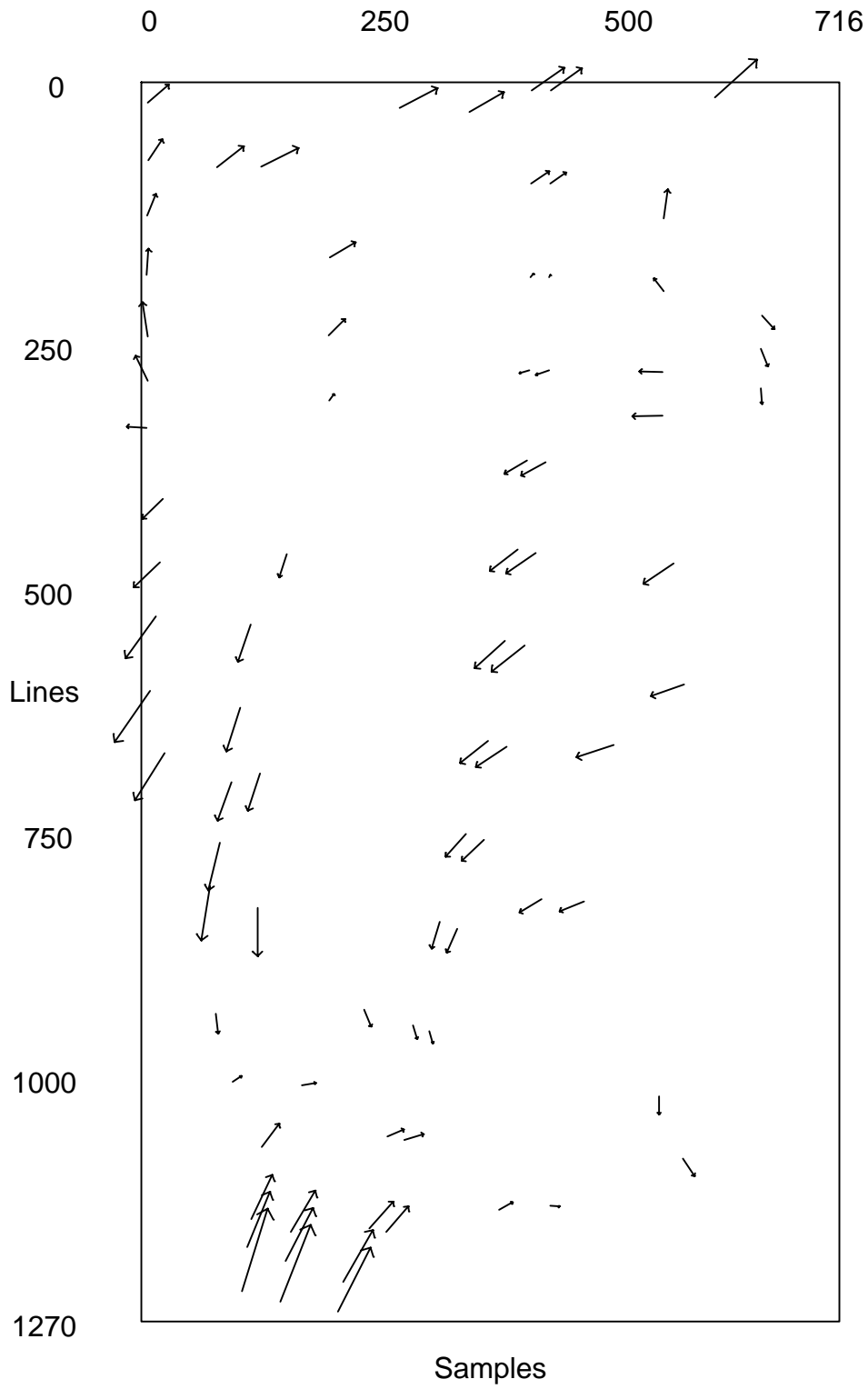


Figure 4-1: First Order Polynomial Model. Inverse Transformation. Displacement Vectors. Input (Distorted) Space.

Polynomial Registration

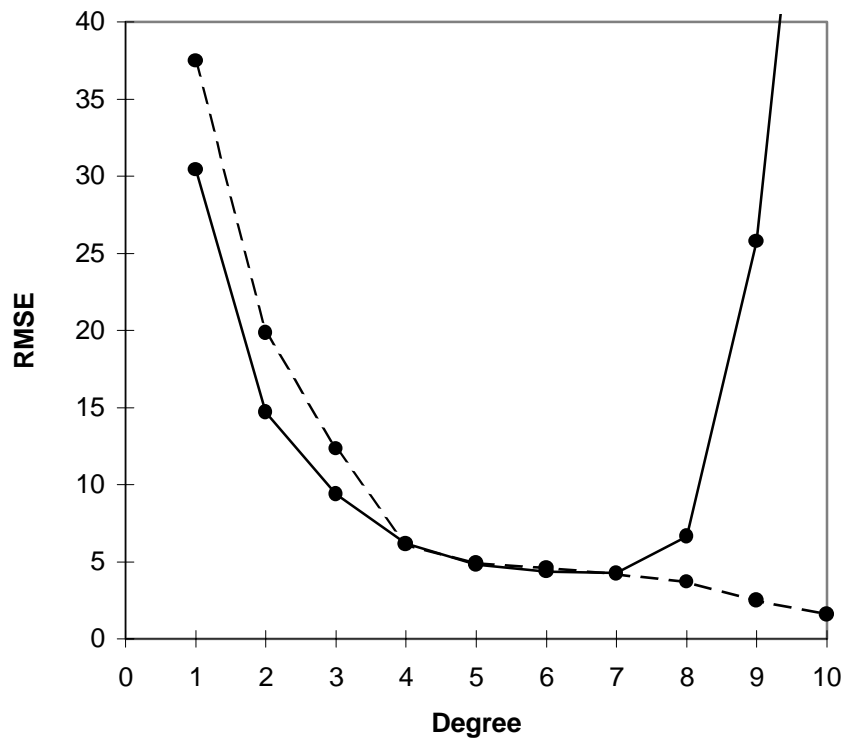


Figure 4-2: Bivariate Mapping Polynomial. RMSE for 83 control points and 27 check points for polynomials of orders one to ten.

Table 4-1 shows the RMSE for the control points. Higher order polynomials result in a lower RMSE, but not necessarily a better distortion model. This is not merely conjecture as shown by Table 4-2. The excursions which characterize polynomials are minimal with low order polynomials, but increase in magnitude as the polynomial order increases. The point at which this occurs is different for x and y which is to be expected. There is no reason why the distortions should be similar in both directions. A plot contrasting the RMSE for control points versus check points is shown in Figure 4-2.

Finally, the polynomial method has great shortcomings when it comes to extrapolation. The greater accuracy generated by higher order polynomials is greatly diminished in value should any region of interest be outside of the perimeter, or convex hull of control points. This is illustrated by a series of perspective plots in the *Residual Magnitudes* Appendix. In this Appendix, a series of plots serves to illustrate the degree to which higher polynomials more closely approximate the data. The unconstrained behavior of the polynomials beyond the convex hull is obvious, whereas the excursion between the control points is not readily apparent. The plots in this Appendix illustrate the manner in which higher-order polynomials approximate more complicated distortion patterns such as those found in the test imagery.

Polynomial Degree	RMSE -- Control Points		
	<i>x</i>	<i>y</i>	<i>Total</i>
1	22.179	30.179	37.452
2	7.979	18.164	19.839
3	3.569	11.807	12.335
4	1.934	5.806	6.120
5	1.509	4.666	4.904
6	1.260	4.421	4.597
7	1.083	4.061	4.203
8	0.604	3.626	3.676
9	0.457	2.455	2.497
10	0.299	1.554	1.582

Table 4-1: Polynomial registration. 83 control points

Polynomial Degree	RMSE -- Check Points		
	<i>x</i>	<i>y</i>	<i>total</i>
1	22.750	20.168	30.402
2	8.285	12.116	14.678
3	3.868	8.549	9.383
4	2.600	5.632	6.203
5	2.341	4.187	4.797
6	2.407	3.623	4.349
7	2.370	3.560	4.277
8	1.881	6.348	6.621
9	7.689	24.576	25.750
10	10.323	68.148	68.925

Table 4-2: Polynomial registration. 27 check points.

4.3.2 Finite Element Method

CAGIS software from RAND Corp. was used to evaluate the finite element method. The CAGIS software automatically grids the data based upon an initial triangulation introducing error into the distortion model. The fineness of the grid determines how much error is due to gridding and how much exists due to nonlinear distortions within the finite elements, *i.e.* within the triangles. There are two options for the tessellation of the control points: (1) Greedy triangulation and (2) Delaunay triangulation (the dual of Thiessen polygons in the graph-theoretic sense). The tables which follow illustrate both the effect of different

triangulations as well as the error introduced by the gridding process. The gridding effect was evaluated by writing a new CAGIS routine. The routine was checked manually for a subset of points to ensure its accuracy. We note that the existing bilinear interpolation uses a double-precision Gauss-Jordan solver. This same CAGIS "utility" program was used for the RMSE evaluation.

There are also two illustrations in the *Residual Magnitudes* Appendix which illustrate the "tin-sheeting" of the finite element method. The linear patches which compose the finite element surface result in a composite surface which has discontinuous first derivatives. This is shown by the sharp edges in the model of the complex distortions. The distortion model can be improved visually and quantitatively only through the addition of new control points.

4.3.2.1 Greedy Triangulation

Table 4-3 shows the results from using the Greedy triangulation and three different grid resolutions. The most obvious result is surprising. The resolution of the grid did not noticeably improve the accuracy of the registration. The total RMSE actually increased slightly. We attribute this effect to computational problems associated with approximating over the long, narrow triangles which sometimes result from the Greedy triangulation.

Another interesting observation is with respect to the gridding effect. It is quite evident if the grid is not dense enough as shown in Table 4-4. The transformed image will appear even less smooth than a standard piecewise linear model over triangles. This can further underscore the presence of nonlinear distortions in the image. It also suggests that the need for diagnostic procedures to identify the appropriate resolution of the grid as opposed to trial-and-error using varying grid sizes. Regardless, it is apparent that the Greedy triangulation may not be well-suited for rapidly varying distortions such as those which on occasion confound the registration of airborne imagery. The potential for missing surface variations appears to be a problem. Table 4-5 lists the RMSEs using all of the ground control points.

Finite Element	RMSE -- Check Points		
Grid	<i>x</i>	<i>y</i>	<i>total</i>
30x30	2.741	4.491	5.261
120x120	2.555	4.789	5.428
360x360	2.569	4.788	5.434

Table 4-3: Finite element. Greedy triangulation. 83 control points and 27 check points.

Finite Element	RMSE -- Grid Points		
Grid	<i>x</i>	<i>y</i>	<i>total</i>
30x30	1.428	3.911	4.164
120x120	0.640	1.740	1.854
360x360	0.296	1.139	1.177

Table 4-4: Finite element. Greedy triangulation. Gridding effect. 83 control points.

Finite Element	RMSE -- Grid Points		
Grid	<i>x</i>	<i>y</i>	<i>total</i>
30x30	1.783	3.490	3.919
120x120	0.737	1.548	1.714
360x360	0.236	0.992	1.019

Table 4-5: Finite element. Greedy triangulation. Gridding effect. 110 control points.

4.3.2.2 Delaunay Triangulation

The "Thiessen" option in CAGIS generates a Delaunay triangulation. Thiessen polygons and Delaunay triangulations have been the subject of a great deal of research. Aurenhammer (1985) provides an overview of the Voronoi diagrams, as computational geometers call Thiessen polygons, and the dual of the planar Voronoi diagram--the Delaunay triangulation. Perhaps the most important observation to make to understand the importance of a Delaunay triangulation is the fact that "extreme" angles are avoided. This is useful for computational reasons as well as the fact that compact triangles will seemingly capture local scene variations. However, the triangulation is surface-independent so that better results are not guaranteed.

Finite Element	RMSE -- Check Points		
Grid	<i>x</i>	<i>y</i>	<i>total</i>
30x30	4.278	2.094	4.763
120x120	4.681	1.792	5.012
360x360	4.681	1.787	5.010

Table 4-6: Finite element Delaunay triangulation. 83 control points and 27 check points.

The Delaunay triangulation improved the total RMSE by almost 0.5 pixels as shown in Table 4-6. This is consistent with what one might expect. The Delaunay triangulation is shown in the Appendix (ASPRS/ACSM '94). There is still a major problem with the gridding effect. It is clear that to improve upon the finite element method, there must be data (or scene dependent triangulations) or a way of generating smoother surfaces which capture some of the local variation, for example, Akima's method (Akima 1978a, 1978b and 1984). In the case of badly warped airborne scanner data, registration using gridding may not be very appropriate. An unexpected outcome from the gridding process is its potential usefulness for distortion diagnostics. The gridding effect, see Table 4-7, is highly local and given a large RMSE, indicative of the need to collect additional control points for linear piecewise warping. Table 4-8 lists the RMSEs using all of the ground control points.

Finite Element	RMSE -- Grid Points		
Grid	<i>x</i>	<i>y</i>	<i>total</i>
30x30	1.275	3.488	3.714
120x120	0.469	0.986	1.092
360x360	0.165	0.721	0.740

Table 4-7: Finite Element. Delaunay triangulation. Gridding effect. 83 control points.

Finite Element	RMSE -- Grid Points		
	<i>x</i>	<i>y</i>	<i>total</i>
30x30	1.654	3.181	3.586
120x120	0.648	0.927	1.131
360x360	0.135	0.628	0.643

Table 4-8: Finite Element. Delaunay triangulation. Gridding effect. 110 control points.

4.3.3 Multiquadric Results

A series of images were created using the MQ method as implemented by Flottesch (1993) and adapted by Fogel (1994, 1995). As noted previously, the MQ has a smoothing factor which may be used to influence the shape of the interpolated surface. The best surface via the multiquadric method may be approximated by using a subset of the control points to "tune" the fit. In this case, we simply used the control points to specify the surface and the check points to find the lowest RMSE which may be used as the best MQ parameter. The MQ parameter is expressed as a product of Göpfert's *G* and the minimum distance squared between the output space control points (Equation 4-2). The results from the MQE software as adapted by Fogel (1995) are presented in Table 4-9.

Multiquadric Method		RMSE		
Polynomial	Göpfert's <i>G</i>	<i>x</i>	<i>y</i>	<i>total</i>
1	2.25	2.056	2.047	2.902
2	2.90	1.898	2.416	3.072
3	2.00	1.777	2.401	2.987
4	1.50	1.647	2.287	2.819
5	1.70	1.659	2.222	2.773

Table 4-9: Multiquadric method. MQE. 83 control points and 27 check points.

The removal of the global trend surface uses a low degree polynomial as listed in the first column. The polynomial fit approximates the correction surface whose residuals are then fitted using the MQ approach. The difference in the MQ parameter across polynomial orders results from the different surfaces which are generated through each set of control points. The slight increase in the RMSE for *y* is a result of the MQ parameter being tuned for the *total* RMSE. The image registration problem involves two surface fitting problems. It is clear that the RMSE could probably be reduced for *y* by using a different MQ parameter for *x* and *y*. The total RMSE would be lower as well. This change may not always generate an improvement in the registration accuracy; the correct distortion model is problem dependent.

The *Residual Magnitudes* Appendix contains an illustration which shows the nature of the multiquadric method as it accommodates local variations. This figure should be compared to the polynomial approaches which were shown to be inadequate for modeling high-frequency distortions. The multiquadric method is also interpolating; it honors the locations of the control points during the transformation.

The evaluation of the MQE included a computational review to ensure that the program was coded correctly. In the 1994 report, we reported discrepancies in the RMSE calculations. S-Plus showed noticeable differences in the RMSE than reported from MQE. At that time, we attributed these differences to the numerical routines used to solve the multiquadric system of equations (numerical precision) or errors in coding. We did not identify the source of the discrepancies. As is the case with trend surface polynomials, the

solution to the multiquadric method, and radial basis functions in general is complicated by high condition numbers in the basis.

Subsequent software development revealed that a combination of factors were responsible for the inconsistencies. These have been remedied for this 1995 report. As stated in the earlier version, a fully operational implementation should include a scaling of (u,v) to the unit square. See, for example, Barrodale, Skea *et al.* (1993), Carlson and Foley (1991) and Kansa (1990a and 1990b).

4.3.4 Thin Plate Splines

The use of thin plate splines was not specified for this report. However, as noted previously, thin plate splines and multiquadric functions are both radial basis functions. For a nominal effort, we can substitute the TPS basis for the MQ and implement the corresponding equilibrium conditions and solve the warping problem. The nature of the TPS is such that the distribution of the control points may not need a preliminary polynomial warp. The plate is forced to bend in such a way that it interpolates the control points, but it is constrained with respect to its local and global curvature. Accordingly, the spacing of the control points may not be as crucial for image warping. The results are presented below in Table 10. The MQ method was applied to the residuals after first applying a least squares affine fit. The TPS was applied directly to the original control points. We do not wish to draw conclusions from this Table, but simply wish to draw attention to the potential of the TPS for image warping. As mentioned previously, the MQ method is more flexible and may yield better surface fitting models. Franke (1982) has implemented TPS with tension (similar, but not equivalent to the MQ tension-like parameter) which is yet another method meriting further investigation.

Radial Basis Functions			RMSE		
	Polynomial	Göpfert's G	<i>x</i>	<i>y</i>	<i>total</i>
MQ	1	2.25	2.056	2.047	2.902
MQ Linear Precision	Not applicable	2.25	2.086	2.036	2.914
TPS	Not applicable	Not applicable	1.874	2.089	2.806

Table 4-10: MQ (no polynomial precision), MQ (linear precision) and TPS (linear precision by default). 83 control points and 27 check points.

The thin plate spline includes linear precision by definition. For the comparison above, we removed the first order trend using an affine least squares fit. In the first case, the previously reported MQ results are listed. This MQ formulation had no polynomial precision. In the second case, the MQ formulation included the polynomial precision of degree one. Experience with the linear precision MQ method without a preliminary polynomial model to remove trend(s) in the data has shown it be less effective for image warping.

4.4 Discussion

It is clear from the results in the previous section that the multiquadric is worthy of additional study for improved image registration. The test case was badly warped imagery over a relatively flat surface. A more robust series of tests should be conducted to examine such distortions as relief displacements, etc. In comparison to the results from S-Plus, the best results from the polynomial and finite elements differed in total RMSE by more than 2 and 1 pixels, respectively. The thin plate spline performed similar to the MQ method, which makes it clear that radial basis functions offer an improvement to existing technology for the image registration problem.

A series of images are presented in the *Warped Images* Appendix which reproduce visually the quantitative results of the preceding sections. These serve to further illustrate the potential of radial basis functions to produce better distortion models than either the polynomials or finite element method.

5 Conclusions

This section contains conclusions based primarily on the theoretical discussion of the surface fitting models and the results of the empirical study. We present a series of observations on current practice and commercial solutions to the registration problem. Finally, there is a section on implications for future research.

5.1 Control Points

The selection of control points is an important component in distortion modeling. This paper has focused on image-to-image registration and therefore we have avoided the use of the expression “ground control points” when referring to reference points for warping (Ground control points imply that locational information for a point in an image is associated with a known map position). The following comments and observations apply to both image-to-map transformations as well as image-to-image transformations.

- A high RMSE for a control point indicates either a bad point or a poor model fit.

It is common practice to consider high control point RMSE to be an indicative of a bad match between corresponding points in the reference and distorted images. In fact, that may be true. However, in the presence of rapidly varying distortions, there is also the possibility that the distortion model has failed to capture complicated patterns of internal and external effects. In the case of airborne scanner data, there is a strong likelihood that a high RMSE may also be due to the presence of terrain and/or sensor-platform effects.

- Control point RMSE inadequately measures model performance.

This statement should be self-evident. There is a need to use other techniques such as ordinary cross-validation to more fully investigate systematic and random patterns of distortions due to internal and external effects. Scientific visualization techniques should be investigated as well to aid the registration process. Morphometrics are a possibility.

The problem of verifying the accuracy of a model has an analog in the remotely sensed data classification process. It is well-known that the a training sample data should not be used to explain classification accuracy. Independent test sites must be used to validate the results with quantitative statements.

5.2 Surface Fitting Models

The use of surface fitting models for image registration will continue to be an important tool for environmental remote sensing. At present, the tools which are available to the remote sensing analyst are those which were developed at a time when computational efficiency was a criterion for implementation. Improvements in computing hardware and subsequent research in scattered data interpolation, surface fitting, computational geometry, computer graphics and numerical analysis make it possible to improve upon current practice. Indeed, the conventional way in which the image warping problem is approached should be reconsidered.

An additional issue in surface fitting analysis for image registration is the use of local vis-à-vis global models. It is clear from our research that some global models may compete with local models in the presence of rapidly varying unsystematic distortions. Comments on this issue are made with respect to the models themselves in the following sections on the polynomial, finite element, and multiquadric methods.

5.2.1 Bivariate Mapping Polynomials

It has been demonstrated that the standard polynomial functions found in commercial image processing systems are not entirely up to the task of modeling complicated distortions found in airborne scanned imagery. In fact, the use of approximating polynomial expressions may not be suitable for satellite imagery either when geometric and radiometric fidelity is at a premium.

We do not advocate abandoning the use of polynomials for image registration. The model's mathematical simplicity and speed of computation may be decidedly advantageous in some cases. It is also accessible to the non-specialist in image warping. The level of geometric correction required is clearly dependent on the nature of the application. With this in mind, the follow statements can be made:

- Bivariate mapping polynomials are a global registration method.
All of the control points are used to construct a single distortion model. Local variations within an image limit the usefulness of the polynomial approach.
- Bivariate mapping polynomials have limited utility for highly distorted images.
In the presence of complicated distortions, conventional application of polynomials for image registration cannot achieve the registration accuracy of interpolating methods. The primary justification for the continued use of polynomials is their simplicity in theory and implementation; accurate registrations, however, will usually require a piecewise or segmented application to scanner imagery.
- The image registration problem involves fitting both an x and a y surface.
The surface fitting approach to image warping is in fact two problems. The distortion models are mutually independent. Conventional practice is to use the same model for x and y , despite the fact that there are two surface fitting problems. Effectively, this represents a compromise between best x -correction and best y -correction. Indeed, it is possible that neither the best model for x nor y will be selected in favor of minimizing total RMSE.
- Weighted polynomials merit investigation.
This report did not address in detail the use of weighted polynomials (a global method) or the local weighted mean technique (a local method). Mathematically, weighted polynomials are not much more complicated than the power series polynomial form discussed in this report. Many of the disadvantages of using polynomials remain, especially in the approximating circumstances.
The local weighted mean technique, like the weighted polynomial, is not mathematically difficult. It is a local method, which offers obvious advantages in the presence of local distortions, but it is more difficult to implement operationally. Local weighted mean

implementation issues are analogous to the image mosaicking problem, *i.e.* a set of images is merged into a single larger image.

It should be clear that the use of polynomial expressions for image registration is still an open research topic in the context of developing a “best” distortion model. At the same time, it cannot be overstated that conventional commercial implementations of polynomials fall well short of being optimal techniques.

5.2.2 Finite Element Methods

In the presence of badly warped imagery, the finite element method has been the only widespread alternative to using bivariate mapping polynomials. The finite element approach in its present form, *e.g.* in VICAR/IBIS and CAGIS, uses a piecewise linear interpolation is used to warp imagery. The local nature of the piecewise transformations means that local distortions will not confound the registration process as a whole. However, nonlinearities between the control points remain a problem. The following general statements may be made:

- The Finite Element Method is a local registration technique.

Only those control points defining each finite element, or surface patch are used to model the distortions for that region. Local variations do not *directly* affect the registration of the entire image. We elaborate this comment in the next statement.

- Control point tessellations impact the overall fit of the Finite Element Method.

There are many possible triangulations of the control points from which we can define a warping model. The distortions in the image are not always well understood prohibiting the choice of a best triangulation. There is good reason to explore the application of data-dependent triangulations as well as interactively specified triangulations where known breaklines exist (*e.g.*, a cliff). The contouring literature may be useful for this purpose.

The fact that a tessellation is independent of the variations in the input image essentially ignores important information that might help better characterize the warp. The best triangulation for image warping will be data-dependent.

- Finite elements may not be merely continuous in value, but smooth as well.

The piecewise linear interpolation over triangles yields a surface which is continuous in value, but not necessarily smooth across triangle boundaries (known as a C^0 surface). Visually, the corrected surface may appear angular at the triangle boundaries. For this reason, linear piecewise modeling is frequently referred to as tin-sheeting as opposed to rubber-sheeting as in the case of polynomials (and the radial basis functions).

Piecewise models which have continuous first partial derivatives appear smoother and are known as C^1 surfaces. As noted in the text, Parr and Comer fitted a fifth order polynomial across the surfaces using Akima's method (1978a and 1978b). This solution may lead to artifacts given the high order of the polynomial (Comer, 1994). Lower order functions, such as cubic interpolation (Goshtasby, 1987) and bicubic interpolation (Renka and Cline, 1984) may offer more satisfactory solutions.

- Extrapolation beyond the convex hull of control points is an open research issue.

The technique used by VICAR/IBIS and CAGIS for extrapolating beyond the convex hull is adequate in most cases for satellite imagery: four corner points are added to the control point coverage far off in the distance. An alternative would be the extension of the exterior region into triangles and quadrilaterals. This would yield a more local solution for extrapolation outside the control points.

Due to the nature of airborne scanned image acquisition, this is not as critical an issue. In the linear case, as long as the convex hull surrounds the area of interest, *i.e.* the study area is

contained within a larger image, it will be unnecessary to consider extrapolation. For C^1 surfaces, nearby control points are used in the surface construction such that the location of control points outside of the convex hull is an important issue.

5.2.3 Radial Basis Functions

The development and implementation of new techniques for image warping is clearly warranted for improved accuracy for environmental monitoring. The tools commonly employed by remote sensing analysts were adequate when alternatives did not exist. In this report, we have shown that alternatives exist, albeit at a cost of increased theoretical and computational complexity. It is our purpose in this section to review those features of the multiquadric method and thin plate splines (radial basis functions) such that it is clear that existing solutions are not the best or only available solutions to image registration. The following comments are relevant:

- Radial Basis Functions are global methods.

All of the control points are used to construct the distortion models. Both techniques may be adjusted to accommodate local variations. The multiquadric parameter may be used to adjust the shape of the surface and improve the distortion modeling. The theoretical characteristics of the thin plate spline may not allow the same degree of flexibility in defining the x and y surfaces (see, for example, Franke, 1985).

- The Multiquadric Method (and Thin Plate Spline) may be applied locally.

The multiquadric provides a well-behaved surface which may be exploited for segmented image registration. The potential application of the multiquadric method for mosaicking can be inferred from work by Schiro and Williams. The barrier to mosaicking is with respect to the difficulties in operationalizing the procedure. Discontinuities in the functions across the “sub-images” will need to be addressed. Franke (1982) discusses the analogous situation for thin plate splines.

Breaking the registration process down into stages using sub-images or using the multiquadric method for mosaicking is still a matter of fitting a global model. The option of breaking down a large image registration project into smaller constituent parts is simply an option which needs to be recognized. Polynomials are unsuitable for this task and the finite element method does not always produce an acceptable warp given severe distortions.

- There may be two best multiquadric parameters: one for x and one for y .

The two surface fitting problems may result in two different distortion models. In the current implementation, this would mean different order polynomials as well as different values for the multiquadric parameter. This point highlights the significance characteristic of the warping problem, *i.e.* we are concerned with the interpolation of scattered data values. The distribution of these values impacts the fit of all of the distortion models. The multistage implementation of the geometric correction component of the warping process is flexible such that there exists no universally best model; digital image registration is a complex topic.

- The Multiquadric Method (and Thin Plate Spline) is computationally intensive.

It is true that the Multiquadric Method is more expensive computationally than either using polynomial power series or the finite element method. A trade-off must be realized wherein registration accuracy and choice of methodology is dependent on the nature of the application.

The gridding approach used in CAGIS, and described in this report, may be used with the polynomial, multiquadric and thin plate splines. This may yield an acceptable alternative to conventional practice wherein the polynomials approximate true locations, but model more

complex distortions than the finite element method. And the finite element method, as currently implemented, does not model nonlinear distortions between the control points. The ability of the Multiquadric method to model complex distortions in a well-behaved fashion, make it a candidate for fast registration via gridding using bilinear functions as in the CAGIS program IMWARP.

Finally, it must be noted that the fast evaluation of radial basis functions is a contemporary research topic which may lead to improvements in the computational requirements (see Beatson and Newsam, 1992). Barrodale, Skea *et al.* have implemented work by Powell for the thin plate spline making it competitive to existing practice. Improvements in registration accuracy for change detection, etc., certainly merit additional overhead if we are to base science and major policy decisions on the results.

5.3 Recommendations

The technical review of the methods described in this report combined with the experimental application make it clear that existing procedures must be augmented by new methods. The complex patterns of airborne scanned imagery distortions motivated this research. It is clear that radial basis functions legitimately merit further investigation. In particular, the multiquadric method performed extremely well in the test case. The similar success with thin plate splines reported by Barrodale *et al.* is consistent with our findings.

The ability of the multiquadric method to deal with large distortions does not mean its application should be limited to airborne acquired imagery. Satellite imagery may be more accurately registered as well. In both cases, the development of more informative diagnostics than the RMSE measure, *e.g.* visualization techniques, will aid in the selection of the most appropriate warping model.

We also note that the possible range of distortions in an image is a function of the internal and external sensor effects and terrain effects. The ability to more accurately model complex distortion patterns using the Multiquadric Method could conceivably aid the process of automated control point extraction. In particular, ephemeris sensor and platform data in combination with a flexible surface fitting model, could guide the extraction process. We make these comments recognizing that the control point extraction process is complicated. Indeed, the identification of a similarity metric which is robust across sensors and seasons is also an open research question.

Finally, we feel it is extremely important to point out that current approaches to image registration are largely constrained by the tools which have been made available by commercial image processing vendors. It is critical that the remote sensing community recognizes and conveys to vendors the essential need for improved registration techniques. Accurate image registration is fundamental to any analysis involving multiple sets of imagery (*e.g.*, change detection and multitemporal classification) or the integration of remote sensing and geographic information system databases.

References

- Akima, H. 1978a. A method of bivariate interpolation and smooth surface fitting for irregularly distributed data. *ACM Transactions on Mathematical Software* 4(2): 148-159.
- Akima, H. 1978b. Algorithm 526, bivariate interpolation and smooth surface fitting for irregularly distributed data [E1]. *ACM Transactions on Mathematical Software* 4(2):160-164.
- Akima, H. 1984. On estimating partial derivatives for bivariate interpolation of scattered data. *Rocky Mountain Journal of Mathematics* 14(10): 41-52.
- Arad, N., N. Dyn, D. Rosenfeld and Y. Yeshurin. 1994. Image warping by radial basis functions: application to facial expressions. *CVGIP: Graphical Models and Image Processing* 56(2): 161-172.
- Aurenhammer, F. 1991. Voronoi diagrams—A survey of a fundamental geometric data structure. *ACM Computing Surveys* 23 (3): 344-405.
- Barnes, S.L. 1995. Comments on "Use of Multiquadric Interpolation for Meteorological Objective Analysis." *Monthly Weather Review* 123(7): 2255-2256. [See Nuss and Titley, 1994]
- Barrodale, I., R. Kurahawa, R. Poeckert and D. Skea. 1993. Side-scan sonar image processing using thin plate splines and control point matching. *Numerical Algorithms* 5: 85-98.
- Barrodale, I., D. Skea, M. Berkley, R. Kurahawa and R. Poeckert. 1993. Warping digital images using thin plate splines. *Pattern Recognition* 26(2): 375-376.
- Beatson, R.K. and G.N. Newsam. 1992. Fast evaluation of radial basis functions: I. *Computer and Mathematics with Applications* 24(12): 7-19.
- Billingsley, F.C. 1983. Data processing and reprocessing. Chapter 17 in (R.N. Colwell, ed.) *The Manual of Remote Sensing, Volume I*. Falls Church, Virginia: American Society of Photogrammetry and Remote Sensing.
- Bernstein, R. 1983. Image geometry and rectification. Chapter 21 in (R.N. Colwell, ed.) *The Manual of Remote Sensing, Volume I*. Falls Church, Virginia: American Society of Photogrammetry and Remote Sensing.
- Bookstein, F.L. 1989. Principal warps: thin plate splines and the decomposition of deformations. *IEEE Transactions on Pattern Analysis and Machine Intelligence* 11(6): 567-585.
- Bryant, N.A. 1981. NASA Workshop on Registration and Rectification. Proceedings of the Nasa Workshop on Registration and Rectification. Pasadena, California, 17-19 November 1981, Jet Propulsion Laboratory, California Institute of Technology, Pasadena, California.
- Carlson, R.E. and T.A. Foley. 1991. The parameter R^2 in multiquadric interpolation. *Computers & Mathematics with Applications* 21(9): 29-42.
- Carlson, R.E. and T.A. Foley. 1992. Interpolation of track data with radial basis function methods. *Computers & Mathematics with Applications* 24(12): 27-34.
- Castleman, K.R. 1979. *Digital image processing*. Englewood Cliffs, New Jersey: Prentice-Hall.
- COSMIC. The University of Georgia, 382 East Broad Street, Athens, GA 30602.
- Cressie, N. 1989. Geostatistics. *The American Statistician* 43(4): 197-202. [See "Comment" by Wahba 1990 and "Reply" by Cressie 1990]
- Cressie, N. 1990. Reply to 'Comment on "Geostatistics."' *The American Statistician* 44(3): 256-258. [See Cressie 1989 and "Comment" by Wahba 1990.]
- Devereux, B.J., R.M. Fuller, L. Carter and R.J. Parsell. 1990. Geometric correction of airborne scanner data by matching Delaunay triangles. *International Journal of Remote Sensing* 11(12): 2237-2251.
- Duchon, J. 1976. Interpolation des fonctions de deux variables suivant le principe de la flexion des plaques minces. *RAIRO, Analyse Numérique* 110: 5-12.

- Dyn, N., D. Levin and S. Rippa. 1990. Algorithms for the construction of data dependent triangulations, pp. 185-192 in (J.C. Mason and M.E. Cox, eds) *Algorithms for Approximation II*. New York: Chapman and Hall.
- Ehlers, M. 1987. Integrative Verarbeitung von digitalen Bilddaten der Satellitphotogrammetrie und -fernerkundung im Rahmen von Geographischen Informationssystemen. Wissenschaftliche Arbeiten der Fachrichtung Vermessungswesen der Universität Hanover, Nr. 149.
- Ehlers, M. and D.N. Fogel. 1994. High-precision geometric correction of airborne remote sensing revisited: the multiquadric interpolation. *Proceedings, SPIE, Image and signal processing for remote sensing*, 26-30 September, Rome, Italy.
- ERDAS/Imagine. ERDAS, Inc. Atlanta, Georgia.
- Flottemesch, U. 1993. Geometrische Entzerrung von digitalen Flugzeugscannerdaten mit der multiquadratischen Interpolation. Diplomarbeit. Institut für Photogrammetrie und Ingenieurvermessungen. Universität Hannover.
- Flusser, J. 1992. An adaptive method for image registration. *Pattern Recognition* 25(1): 45-54.
- Fogel, D.N. 1994. MQE Version 1.20. A computer program. Department of Geography. University of California. Santa Barbara, California.
- Fogel, D.N. 1995. MQReg Version 2.00. A computer program. Department of Geography. University of California. Santa Barbara, California.
- Foley, T.A. 1987. Interpolation and approximation of 3-D and 4-D scattered data. *Computers and Mathematics Applications* 13(8): 711-740.
- Fortune, S.J. 1987. A sweepline algorithm for Voronoi diagrams. *Algorithmica* 2: 153-174.
- Franke, R. 1979. A critical comparison of some methods for interpolation. Technical Report NPS-53-79-003. Naval Postgraduate School, Monterey, California.
- Franke, R. 1982. Scattered data interpolation: tests of some methods. *Mathematics of Computation* 38(157): 181-200.
- Franke, R. 1982. Smooth interpolation of scattered data by local thin plate splines. *Computers & Mathematics with Applications* 8(4): 273-281.
- Franke, R. 1987. Recent advances in the approximation of surfaces from scattered data, pp. 78-98 in (C.K. Chui, L.L. Schumaker and F.I. Utreras, eds.) *Topics in Multivariate Approximation*, Orlando, Florida: Academic Press.
- Franke, R. 1985. Thin plate splines with tension. *Computer Aided Geometric Design* 2: 87-95.
- Franke, R. and G.M. Nielson. 1991. Scattered data interpolation: A tutorial and survey, pp. 131-160 in (H. Hagen and D. Roller, eds.) *Geometric Modeling: Methods and Applications*. Berlin: Springer-Verlag.
- Franke, R. 1994. Personal communication.
- Franke, R., H. Hagen and G.M. Nielson. 1994. Least squares surface approximation to scattered data using multiquadric functions. *Advances in Computational Mathematics* 2: 81-99.
- GNU Project, The. 1995. Free Software Foundation. 675 Massachusetts Avenue. Cambridge, MA.
- Gold, C. 1994. Personal communication.
- Golub, G.H. and C.F. Van Loan. 1989. *Matrix Computations. Second Edition*. Baltimore, Maryland: The Johns Hopkins University Press.
- Göpfert, W. 1977. Interpolationsergebnisse mit der multiquadratischen Methode. *Zeitschrift für Vermessungswesen* 19: S.457-460.
- Göpfert, W. 1982. Methodology for thematic image processing using thematic and topographic data bases and base-integrated multi-sensor imagery. Proceedings, ISPRS Commission VII Symposium. Toulouse, France, 13.

- Goshtasby, A. 1986. Piecewise linear mapping functions for image registration. *Pattern Recognition* 19(6): 459-466.
- Goshtasby, A. 1987. Piecewise cubic mapping functions for image registration *Pattern Recognition* 20(5): 525-533.
- Goshtasby, A. 1988a. Image registration by local approximation methods. *Image and Vision Computing* 6(4): 255-261.
- Goshtasby, A. 1988b. Registration of images with geometric distortion. *IEEE Transactions on Geoscience and Remote Sensing* 26(1): 60-64.
- Hall, E.L. 1979. *Computer image processing and recognition*. New York: Academic Press.
- Harder, R.L. and R.N. Desmarais 1972. Interpolation using surface splines. *Journal of Aircraft* 9(2): 189-191.
- Hardy, R.L. 1971. Multiquadric equations of topography and other irregular surfaces. *Journal of Geophysical Research* 76(8): 1905-1915.
- Hardy, R.L. 1977. Least squares prediction. *Photogrammetric Engineering and Remote Sensing* 43(4): 475-492.
- Hardy, R.L. 1990. Theory and applications of the multiquadric-biharmonic method. *Computers and Mathematical Applications* 19(8/9): 163-208.
- Interactive Data Language. Version 3.1 . Research Systems, Inc. Boulder, Colorado.
- IMSL-Reference Manual, 8th Ed. 1980. IMSL (International Mathematical and Statistical Libraries, Inc.).
- Kansa, E.J. 1990a. Multiquadrics—A scattered data approximation scheme with applications to fluid dynamics—I. Surface approximations and partial derivative estimates. *Computers and Mathematics with Applications* 19: 127-145.
- Kansa, E.J. 1990b. Multiquadrics—A scattered data approximation scheme with applications to fluid dynamics—II. Solutions to parabolic, hyperbolic and elliptical partial differential equations. *Computers and Mathematics with Applications* 19: 147-161.
- Kloer, B. 1994. Personal communication.
- Kratky, V. 1976. Grid-modified polynomial transformation of satellite imagery. *Remote Sensing of Environment* 5: 67-74.
- Lancaster, P. and K. Salkauskas. 1986. *Curve and surface fitting: an introduction*. London: Academic Press.
- Lawson, C. 1977. Software for C^1 surface interpolation, pp. 161-194 in *Mathematical Software III*, John R. Rice, Editor. Academic Press: New York.
- Leckie, D.G. 1980. Use of polynomial transformations for registration of airborne digital line scan images. Proceedings, Sixth Canadian Symposium on Remote Sensing, Ottawa, Canada, Canadian Aeronautics and Space Institute.
- Lingas, A. 1986. The greedy and Delauney [sic] triangulations are not bad in the average case. *Information Processing Letters* 22: 25-31.
- Manacher, G. and A.L. Zobrist. 1979. Neither the greedy nor the Delaunay triangulation of a planar point set approximates the optimal triangulation. *Information Processing Letters* 9(1): 31-34.
- Mather, P.M. 1987. *Computer processing of remotely-sensed images: an introduction*. Wiley: New York.
- Meinguet, J. 1979. Multivariate interpolation at arbitrary points made simple. *Journal of Applied Mathematics and Physics (ZAMP)* 30: 292-304.
- Micchelli, C.A. 1986. Interpolation of scattered data: distance matrices and conditionally positive definite functions. *Constructive Approximation* 2(1): 11-22.
- Mitasova, H. and L. Mitas. 1993. Interpolation by regularized spline with tension: I. Theory and Implementation. *Mathematical Geology* 25(6): 641-655.

- Moik, J. 1980. *Digital image processing of remotely sensed images*. NASA SP-431. Washington, D.C.: NASA.
- Niblack, W. 1986. *An introduction to digital image processing*. Englewood Cliffs, New Jersey: Prentice/Hall International.
- Nielson, G.M. 1987. Coordinate free scattered data interpolation, pp. 175-184 in (C.K. Chui, L.L. Schumaker and F.I. Utreras, eds.) *Topics in Multivariate Approximation*, Orlando, Florida: Academic Press.
- Nielson, G.M. 1989. A characterization of an affine invariant triangulation, *Computing Supplement 8*: 191-210.
- Nielson, G.M. and T.A. Foley. 1989. A survey of applications of an affine invariant norm, pp. 445-467 in (T. Lyche and L.L. Schumaker, eds.) *Mathematical Methods in Computer Aided Design*, Boston: Academic Press.
- Nuss, W.A. and D.W. Titley. 1994. Use of Multiquadric Interpolation for Meteorological Objective Analysis. *Monthly Weather Review* 122(7): 1611-1631. [See "Comment" by Barnes, 1995 and "Reply" by Nuss and Titley, 1995]
- Nuss, W.A. and D.W. Titley. 1995. Reply to 'Comments on "Use of Multiquadric Interpolation for Meteorological Objective Analysis."' *Monthly Weather Review* 123(7): 2257-2259. [See Barnes, 1995]
- Okabe, A., B. Boots and K. Sugihara. 1992. *Spatial tessellations: concepts and applications of Voronoi diagrams*. Chichester, England: Wiley & Sons.
- Parr, J.T. and R.P. Comer. 1990. A local area geometric warping algorithm. Pages 316-20 in Volume 4, *Proceedings of the ACSM/ASPRS Annual Convention*. March 18-23, 1989, Denver, Colorado.
- PCI. 1994. PCI EASI/PACE. Richmond Hill, Ontario, Canada.
- Powell, M.J.D. 1987. Radial basis functions for multivariate interpolation: a review, pp. 143-167 in (J.C. Mason and M.G. Cox, eds) *Algorithms for Approximation*, Oxford: Oxford University Press.
- Powell, M.J.D. 1992. Tabulation of thin plate splines on a very fine two-dimensional grid. Pages 221-244 (Dietrich Braess and Larry L. Schumaker, eds.) *Numerical Methods of Approximation Theory*. Basel: Birkhäuser Verlag.
- Preparata, F.P. and I. Shamos. 1985. *Computational geometry: an introduction*. New York: Springer-Verlag.
- Rippa, S. 1992. Long, thin triangles can be good for linear interpolation. *SIAM Journal of Scientific and Statistical Computing* 13: 1123-114.
- Ruprecht, D. and H. Müller. 1993. Free form deformation with scattered data interpolation methods. *Computing Supplement 8*: 267-281.
- Ruprecht, D. and H. Müller. 1995. Image warping with scattered data interpolation. *IEEE Computer Graphics and Applications* 15(2): 37-43.
- Ruprecht, D., R. Nagel and H. Müller. 1995. Spatial free form deformation with scattered data interpolation methods. *Computers & Graphics* 19(1): 63-71.
- Saalfeld, A. 1985. A fast-rubber sheeting transformation using simplicial coordinates. *The American Cartographer* 12(2): 169-173.
- Sabin, M.A. 1980. Contouring - a review of methods for scattered data, pp. 63-86 in (K.W. Brodlie, ed.) *Mathematical Methods in Computer Graphics and Design*, New York: Academic Press.
- Scepan, J., J. Estes and D. Lanter. 1992. Improved integration of remote sensing imagery with geographic information systems. Remote Sensing Research Unit. Department of Geography. University of California, Santa Barbara.
- Schiro, R. and G. Williams. 1984. An adaptive application of multiquadric interpolants for numerically modeling large numbers of irregularly spaced hydrographic data. *Surveying and Mapping* 44: 365-381.

- Schumaker, L.L. 1987. Numerical aspects of spaces of piecewise polynomials on triangulations, pp. 373-406 in (J.C. Mason and M.G. Cox, eds.) *Algorithms for Approximation*. Oxford: Oxford University Press.
- Schumaker, L.L. 1987. Triangulation methods, pp. 219-232 in (C.K. Chui, L. L. Schumaker and F. Utreras, eds.) *Topics in Multivariate Approximation*. New York: Academic Press.
- Schumaker, L.L. 1993. Computing optimal triangulations using simulated annealing. *Computer Aided Geometric Design* 10: 329-345.
- Shul'min, M.V. and Y.Y. Mitel'man. 1974. The multiquadric method of approximating a topographic surface. *Geodesy, mapping and photogrammetry* 16: 13-17; translated from Russian for AGU, ACSM and ASP (1977).
- Simon, K.W. 1975. Digital image reconstruction and resampling for geometric manipulation. *Proceedings, IEEE Symposium on Machine Processing of Remotely Sensed Data*, 3A-1-3A-11.
- Snoeyink, J. 1994. Personal communication.
- Spiess, E. and C. Brandenberger. 1986. Transformation of digital and analogue map data by interpolation methods--an important tool in small-scale map production. *Internationales Jahrbuch fur Kartographie* 36: 149-174.
- Stewart, D.E. and Z. Leyk. 1994. *Meschach: matrix computations in C*. Canberra, Australia: Australia National University.
- Swartzlander, E.E., Jr., J.Eldon, R.M. Glidden, M.J. Jamgochian and Z.Z. Stroll. 1988. How to transform, interpolate, and improve your image. (TRW Space & Defense Sector) *Quest* Winter(1987/1988): 5-18.
- Tarwater, A.E. 1985. A parameter study of Hardy's multiquadric method for scattered data interpolation. Technical Report UCID-53670. Livermore, California. Lawrence Livermore National Lab.
- Thormodsgard, J. M. and T. Lillesand. 1987. Comparison of the gridded finite element and the polynomial interpolations for geometric rectification and mosaicking of Landsat data. Pages 139-151, Proceedings of the ASPRS-ACSM Annual Convention, Volume 2, Baltimore, Maryland.
- Tobler, W.R. 1994. Bidimensional regression. *Geographical Analysis* 26(3): 187-212.
- Wahba, G. 1990. Comment on "Geostatistics." *The American Statistician* 44(3): 255-256. [See Cressie 1989 and "Reply" by Cressie 1990.]
- White, M.S., Jr. and P. Griffin. 1985. Piecewise linear rubber-sheet map transformation. *The American Cartographer* 12(2): 123-131.
- Wolberg, G. 1990. *Digital Image Warping*. Los Alamitos, California: IEEE Computer Society Press.
- Zobrist, A.L., L.J. Marcellino and G.S. Daniels. 1991. *RAND's Cartographic Analysis and Geographic Information System (RAND-CAGIS): A Guide to System Use*. Santa Monica: Rand Corporation.
- Zobrist, A.L., N.A. Bryant and R.G. McLeod. 1983. Technology for large digital mosaics of Landsat data. *Photogrammetric Engineering and Remote Sensing* 49(9): 1325-1335.
- Zobrist, A.L. 1994. Personal communication.

Appendix A : Las Vegas Images

Distorted Image



Remote Sensing Laboratory Complex. EG&G Energy Measurements, Las Vegas, Nevada. The aircraft in the top center has a wingspan of 105 ft. 4 in. Daedalus AADS1268 Band 7, 0.625-0.695 μm .

Appendix A : Las Vegas Images

Reference Image



Remote Sensing Laboratory Complex. EG&G Energy Measurements, Las Vegas, Nevada. This image was acquired by scan digitizing a color photograph using a Sharp JPX-600 color scanner. The image is 1800 samples by 2400 lines. The first 600 samples of the original scan-digitized product were cropped to produced this graphic. The aircraft in the top center has a wingspan of 105 ft. 4 in.

Appendix B : Control Points and Check Points

Control Points

The following list of control points is based on an upper-left origin. The coordinate (1,1) is in the center of the pixel in the upper-left corner. This is the format used by ERDAS Version 7.5, the system which was used to extract the control points and the check points.

CP	<i>U</i>	<i>V</i>	<i>X</i>	<i>Y</i>
1	1950.250	181.250	400.645	9.121
2	1888.875	374.625	400.125	104.625
3	1828.989	565.580	399.375	200.875
4	1771.034	752.193	398.125	295.875
5	1712.307	940.352	395.625	388.625
6	1654.352	1121.943	385.875	479.875
7	1596.398	1303.534	373.125	573.125
8	1539.216	1480.875	355.625	675.875
9	1483.193	1655.898	333.375	771.375
10	1427.557	1826.670	306.125	861.375
11	1373.080	1995.125	278.625	967.375
12	1319.761	2164.352	252.625	1081.375
13	1278.034	2299.193	234.125	1175.375
14	2391.250	232.750	588.611	16.340
15	2102.250	617.250	535.772	214.989
16	2019.250	874.250	534.617	342.609
17	2002.852	1199.989	545.875	493.625
18	1806.580	1510.239	484.375	679.875
19	1638.125	1788.420	410.875	837.875
20	1550.034	2341.693	367.375	1156.125
21	1007.875	2206.625	112.875	1165.625
22	961.602	2005.557	93.875	1025.375
23	1028.443	1781.080	119.625	846.625
24	1322.824	242.643	122.790	87.405
25	1197.750	220.250	77.875	87.625
26	1014.125	178.875	7.438	80.938
27	985.375	282.125	6.062	137.438
28	955.125	384.375	5.812	198.312
29	927.375	484.875	6.438	261.688
30	898.375	585.375	6.938	306.812

Control Points

CP	<i>U</i>	<i>V</i>	<i>X</i>	<i>Y</i>
31	861.125	718.125	5.562	355.188
32	874.250	900.250	22.312	427.438
33	837.750	1029.250	19.062	492.938
34	801.250	1162.750	15.125	548.125
35	755.750	1320.750	8.875	624.375
36	787.000	1439.000	23.875	688.125
37	919.250	1916.250	76.875	955.125
38	1989.750	188.250	420.279	9.410
39	1927.779	382.871	419.699	104.416
40	1867.092	574.138	418.587	200.438
41	1808.708	761.500	418.087	295.787
42	1749.792	949.392	414.538	390.087
43	1691.319	1132.242	404.788	482.832
44	1633.288	1315.181	393.538	578.087
45	1574.992	1493.254	374.837	681.587
46	1518.731	1668.938	351.688	777.337
47	1462.115	1840.377	324.387	868.138
48	1407.623	2008.985	295.438	973.238
49	1364.277	2180.512	269.587	1084.638
50	1311.023	2314.354	251.188	1179.188
51	2156.250	451.250	535.772	140.495
52	2364.750	755.750	636.875	239.875
53	2340.750	825.750	635.375	273.625
54	2317.750	895.250	635.625	314.125
55	1729.375	1799.375	454.375	840.125
56	1972.125	2355.125	555.625	1103.875
57	1906.250	2224.250	530.875	1040.125
58	1656.625	2366.875	419.375	1152.375
59	989.062	2269.562	103.312	1240.062
60	997.812	2237.812	108.438	1194.688

Control Points

CP	<i>U</i>	<i>V</i>	<i>X</i>	<i>Y</i>
61	1036.312	2110.000	123.812	1092.188
62	1042.875	1498.375	121.875	709.125
63	904.250	1731.250	70.625	824.875
64	932.250	1637.250	80.625	779.875
65	970.250	1506.750	92.562	718.188
66	1008.125	1376.625	101.875	641.875
67	1056.875	1209.125	112.438	556.312
68	1171.875	1060.625	149.062	484.188
69	1042.625	76.375	7.045	21.627
70	1805.125	207.625	336.646	31.238
71	1655.250	176.750	264.945	27.130
72	1386.000	587.500	192.175	260.111
73	1429.000	444.000	193.416	180.077
74	1343.000	728.500	192.796	327.116
75	1991.375	1418.625	557.060	617.706
76	2072.750	705.750	534.617	255.411
77	1270.375	1956.125	228.557	951.248
78	1130.125	2044.375	164.737	1028.808
79	1102.875	2251.875	153.436	1178.832
80	1093.125	2283.875	147.999	1208.964
81	1083.625	2315.625	142.707	1250.268
82	1223.625	2346.625	207.383	1230.278
83	1213.875	2379.625	201.503	1260.704

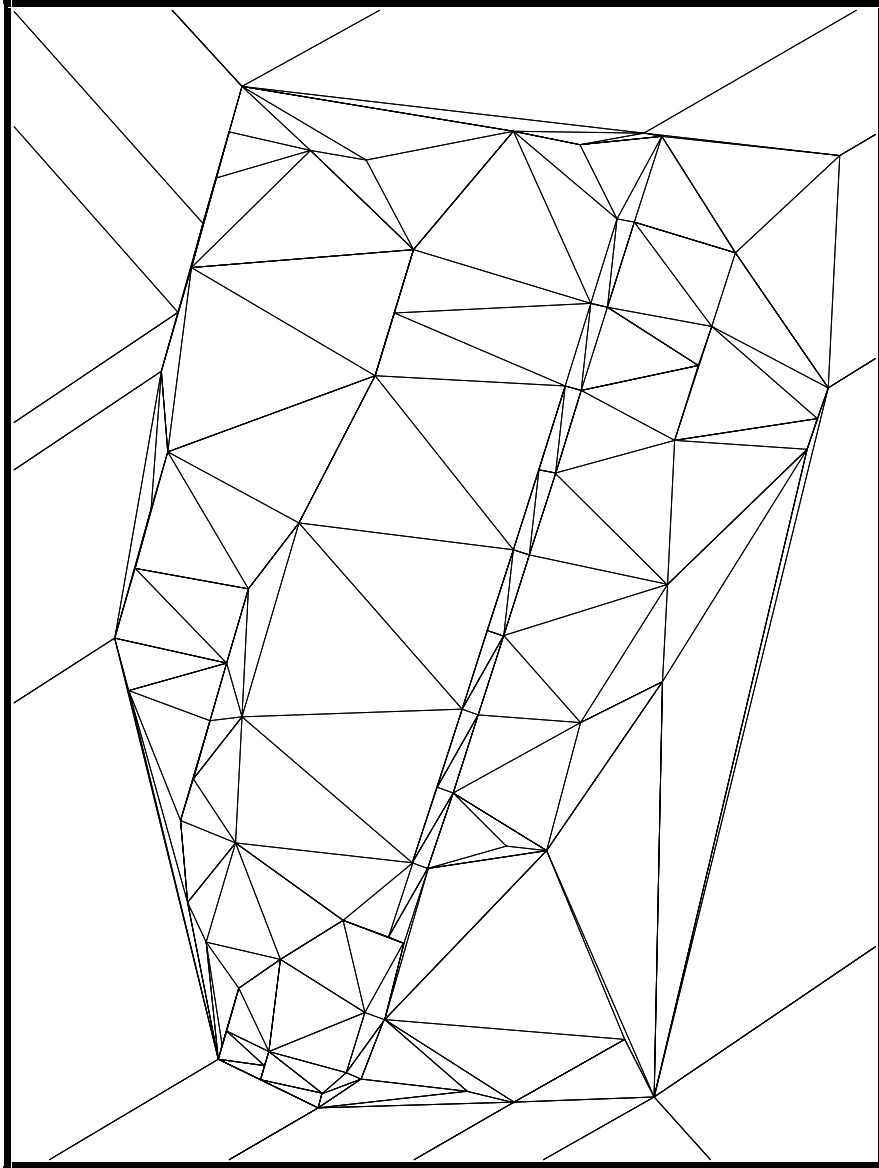
Check Points

The following list of check points is based on an upper-left origin. The coordinate (1,1) is in the center of the pixel in the upper-left corner. This is the format used by ERDAS Version 7.5, the system which was used to extract the control points and the check points.

CP	<i>U</i>	<i>V</i>	<i>X</i>	<i>Y</i>
1	2130.250	529.750	535.483	176.298
2	1843.125	2071.375	502.438	971.812
3	2045.750	790.250	534.906	297.855
4	1569.750	1788.750	376.968	838.654
5	1577.625	1765.625	381.660	827.177
6	1630.125	1811.125	406.058	851.575
7	1393.875	1931.375	289.699	926.790
8	1244.875	2281.125	218.670	1169.471
9	1524.125	2311.375	354.953	1141.464
10	1920.375	1304.375	522.707	555.190
11	2051.375	1180.625	562.985	480.696
12	2146.625	1093.375	590.993	428.435
13	1485.875	1268.375	316.984	562.985
14	1680.625	774.625	360.005	316.118
15	1773.875	507.375	365.347	177.814
16	1806.375	403.125	366.213	125.120
17	1954.125	210.375	406.925	22.475
18	1834.125	252.125	357.262	51.060
19	1409.875	258.875	162.078	88.018
20	1456.125	106.375	162.656	6.017
21	1296.875	643.375	160.635	295.329
22	1278.875	946.375	186.332	420.784
23	1285.625	1170.785	211.885	527.182
24	1235.125	1660.375	211.307	781.701
25	1228.375	2088.625	209.448	1043.208
26	1132.375	2155.375	164.462	1106.219
27	1234.375	2313.625	213.262	1194.853

Appendix C : Triangulations

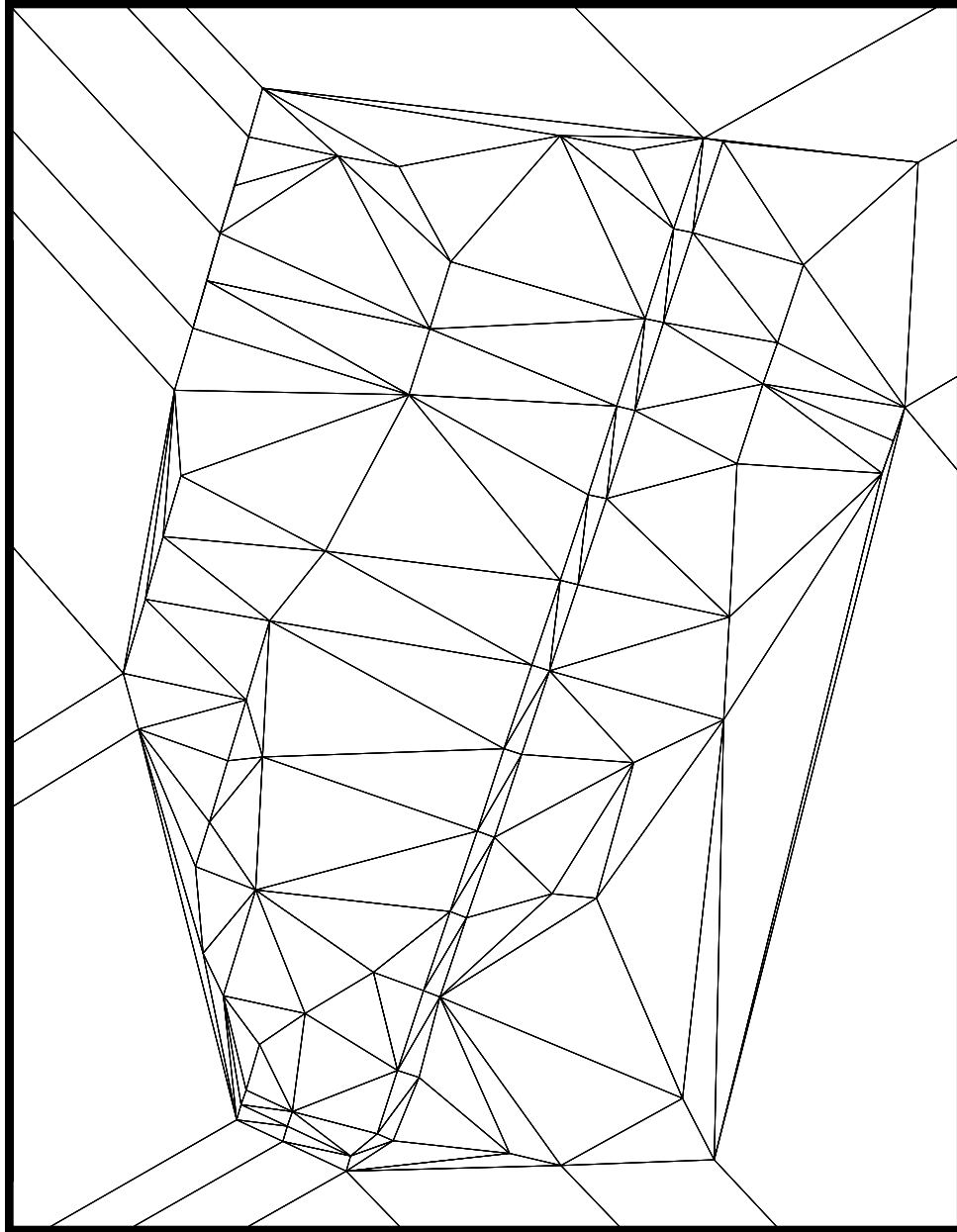
Greedy Triangulation



Greedy Triangulation of Control Points in the Reference Image. The vertices indicate the locations of the control points. Extrapolation outside the convex hull uses four extreme points to complete the triangulation.

Appendix D : Triangulations

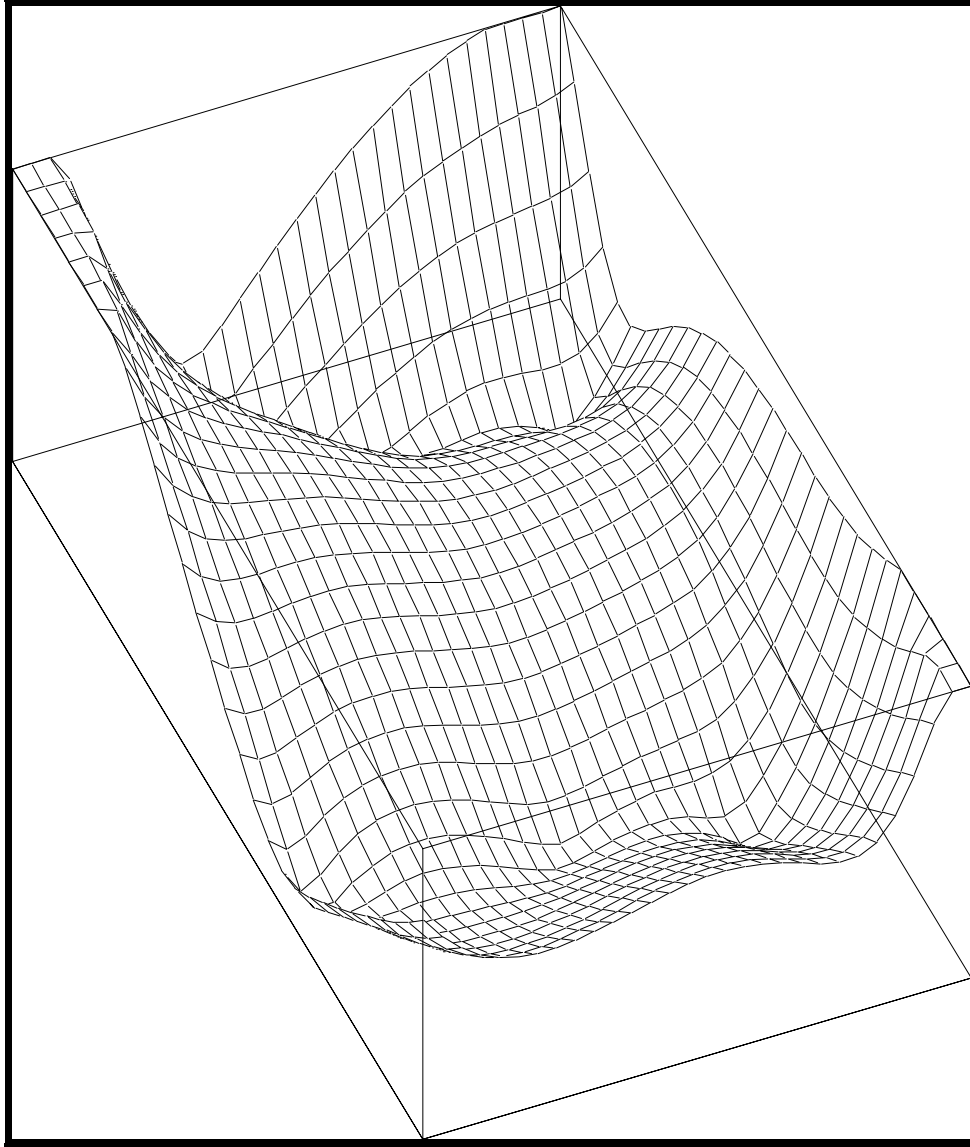
Thiessen Triangulation



Thiessen Triangulation of Control Points in the Reference Image. The vertices indicate the locations of the control points. Extrapolation outside the convex hull uses four extreme points to complete the triangulation.

Appendix D : Residual Magnitude Difference Plots

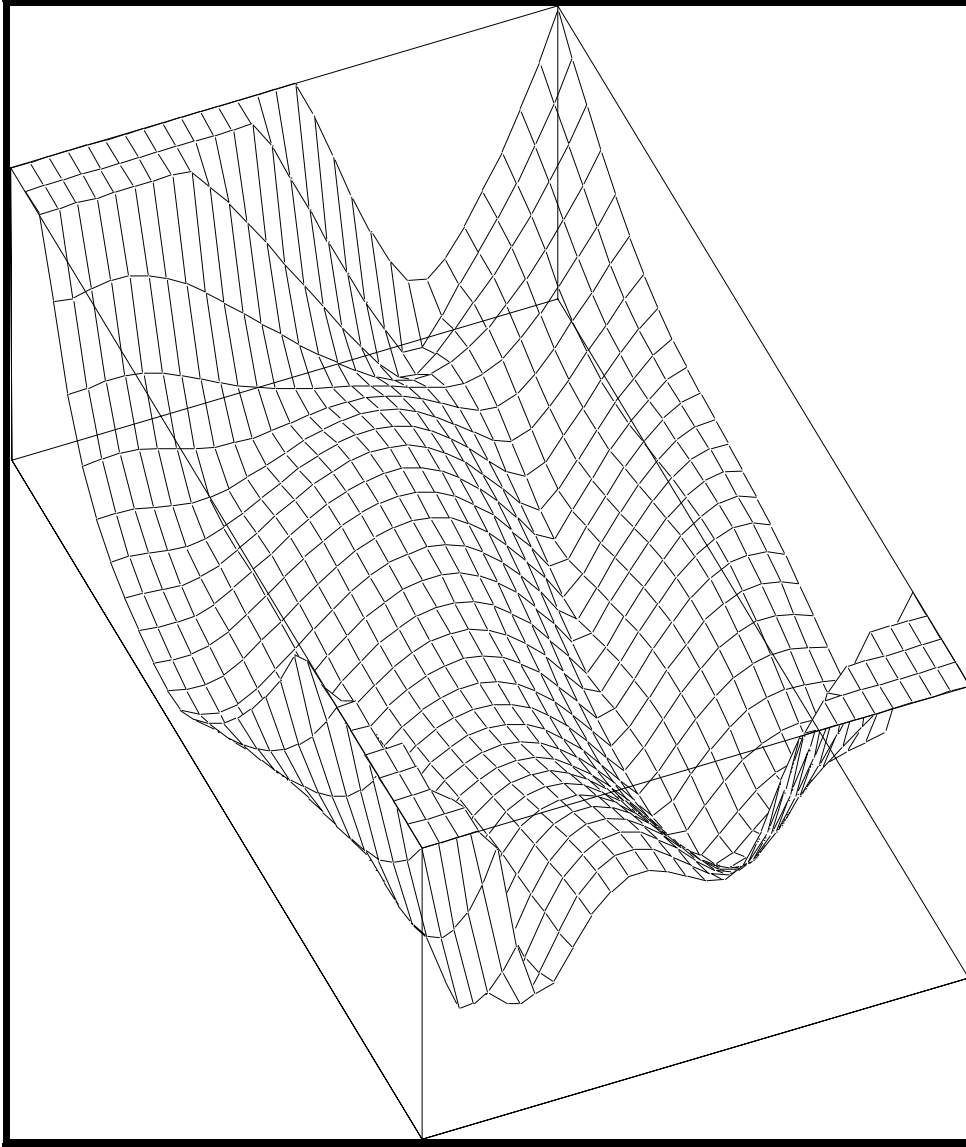
Third Order Polynomial



Perspective view of the magnitude of the difference from a plane between a third order polynomial and a first order polynomial (*i.e.* a least-squares affine transformation). The vertical scale is to 100 pixels RMSE.

Appendix E : Residual Magnitude Difference Plot

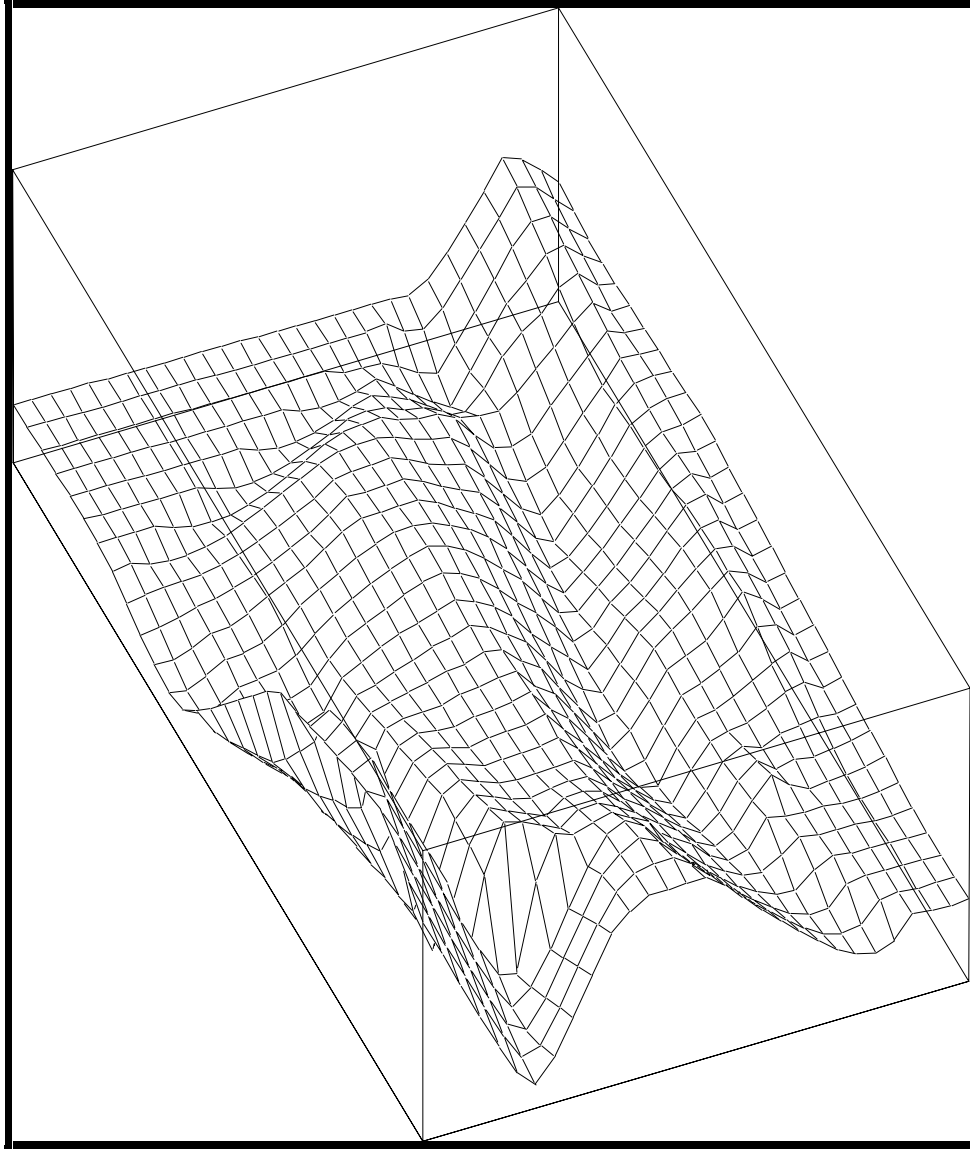
Sixth Order Polynomial



Perspective view of the magnitude of the difference from a plane between a sixth order polynomial and a first order polynomial (*i.e.* a least-squares affine transformation). The vertical scale is to 100 pixels RMSE.

Appendix F : Residual Magnitude Difference Plot

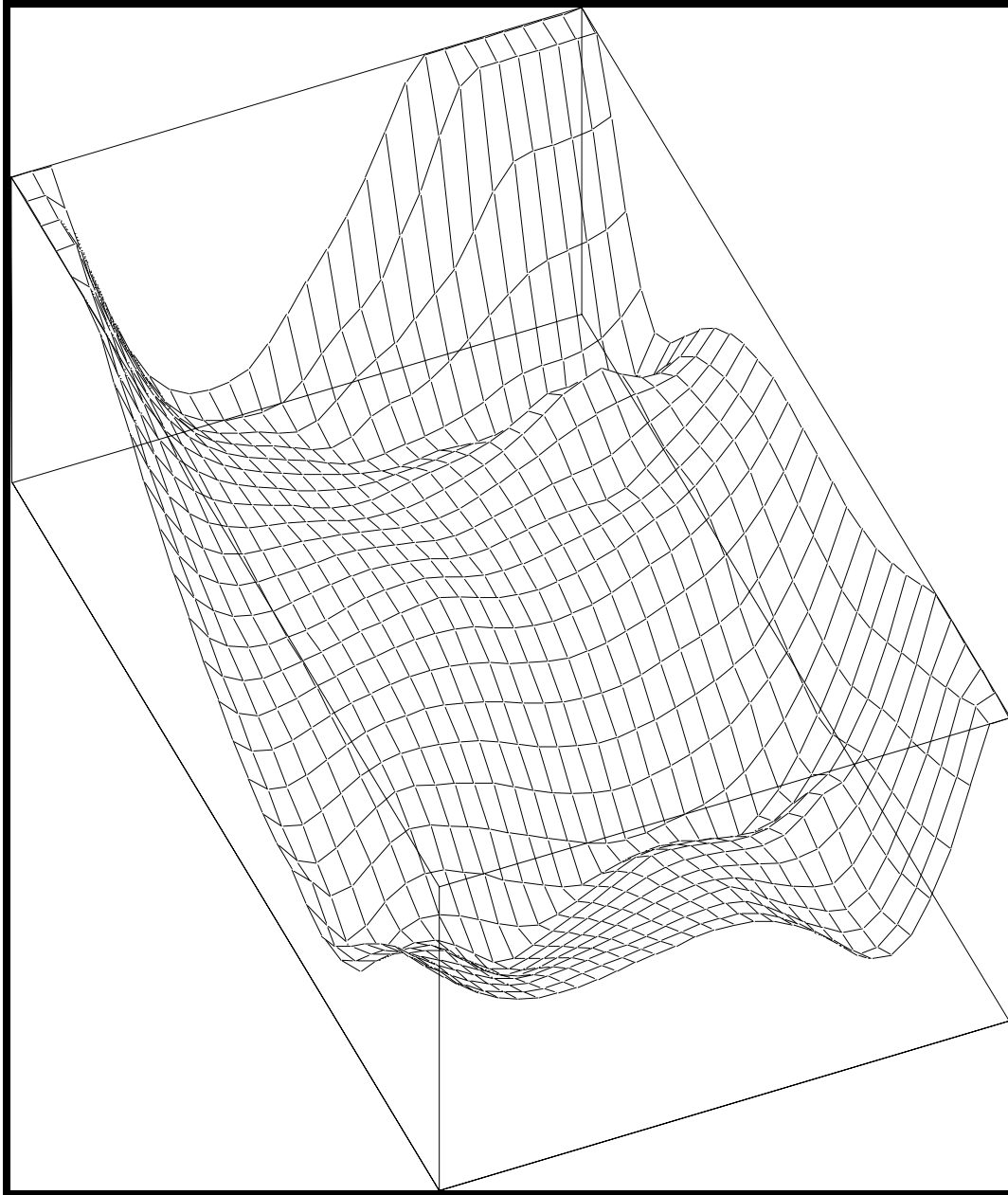
Finite Element Method (30 x 30 Gridding)



Perspective view of the magnitude of the difference from a plane between a piecewise linear model (using a 30x30 grid) and a first order polynomial (*i.e.* a least-squares affine transformation). The vertical scale is to 100 pixels RMSE.

Appendix G : Residual Magnitude Difference Plot

Third Order Polynomial with Multiquadric Method



Perspective view of the magnitude of the difference from a plane between a two-stage model, third-order polynomial and multiquadric method, and a first order polynomial (*i.e.* a least-squares affine transformation). The vertical scale is to 100 pixels RMSE.

Appendix E : Warped Images

First Order Bivariate Mapping Polynomial



First Order Polynomial. Origin (1,1) at the center of the pixel in the upper left corner of the reference coordinate system. Image extents shown here are: upper left (601,1) and lower right (2400,2400).

Appendix E : Warped Images

Third Order Bivariate Mapping Polynomial



Third Order Polynomial. Origin (1,1) at the center of the pixel in the upper left corner of the reference coordinate system. Image extents shown here are: upper left (601,1) and lower right (2400,2400).

Appendix E : Warped Images

Finite Element Method (120 x 120 Gridding)



Finite Element Method. Thiessen Triangulation. Origin (1,1) at the center of the pixel in the upper left corner of the reference coordinate system. Image extents shown here are: upper left (601,1) and lower right (2400,2400).

Appendix E : Warped Images

Two-Stage Multiquadric Method



Third Order Polynomial and Multiquadric Two-Stage Image Registration. Origin (1,1) at the center of the pixel in the upper left corner of the reference coordinate system. Image extents shown here are: upper left (601,1) and lower right (2400,2400).

Appendix E : Warped Images

Two-Stage Reciprocal Multiquadric Method



Third Order Polynomial and Reciprocal Multiquadric Two-Stage Image Registration. Origin (1,1) at the center of the pixel in the upper left corner of the reference coordinate system. Image extents shown here are: upper left (601,1) and lower right (2400,2400).

Appendix E : Warped Images

Thin Plate Method



Thin Plate Spline. Origin (1,1) at the center of the pixel in the upper left corner of the reference coordinate system. Image extents shown here are: upper left (601,1) and lower right (2400,2400).